A&A 488, 1031–1046 (2008)
DOI: 10.1051/0004-6361:200809885

Astronomy & Astrophysics

The photospheric solar oxygen project⋆

I. Abundance analysis of atomic lines and influence of atmospheric models

E. Caffau[1], H.-G. Ludwig[1,2], M. Steffen[3], T. R. Ayres[4], P. Bonifacio[1,2,5], R. Cayrel[6], B. Freytag[7,8], and B. Plez[8,9]

[1] GEPI, Observatoire de Paris, CNRS, Université Paris Diderot, 92195 Meudon Cedex, France
e-mail: Elisabetta.Caffau@obspm.fr
[2] CIFIST Marie Curie Excellence Team
[3] Astrophysikalisches Institut Potsdam, An der Sternwarte 16, 14482 Potsdam, Germany
[4] Center for Astrophysics and Space Astronomy, University of Colorado 389 UCB (CASA), Boulder, CO 80309-0389, USA
[5] Istituto Nazionale di Astrofisica, Osservatorio Astronomico di Trieste, via Tiepolo 11, 34143 Trieste, Italy
[6] GEPI, Observatoire de Paris, CNRS, Université Paris Diderot, 61 Av. de l'Observatoire, 75014 Paris, France
[7] CRAL,UMR 5574: CNRS, Université de Lyon, École Normale Supérieure de Lyon, 46 allée d'Italie, 69364 Lyon Cedex 7, France
[8] Department of Physics and Astronomy, Uppsala University, Box 515, 751 20 Uppsala, Sweden
[9] GRAAL, CNRS UMR 5024, Université Montpellier II, 34095 Montpellier Cedex 5, France

Received 1 April 2008 / Accepted 28 May 2008

ABSTRACT

Context. The solar oxygen abundance has undergone a major downward revision in the past decade, the most noticeable one being the update including 3D hydrodynamical simulations to model the solar photosphere. Up to now, such an analysis has only been carried out by one group using one radiation-hydrodynamics code.
Aims. We investigate the photospheric oxygen abundance considering lines from atomic transitions. We also consider the relationship between the solar model used and the resulting solar oxygen abundance, to understand whether the downward abundance revision is specifically related to 3D hydrodynamical effects.
Methods. We performed a new determination of the solar photospheric oxygen abundance by analysing different high-resolution high signal-to-noise ratio atlases of the solar flux and disc-centre intensity, making use of the latest generation of CO5BOLD 3D solar model atmospheres.
Results. We find $8.73 \leq \log(N_{\rm O}/N_{\rm H}) + 12 \leq 8.79$. The lower and upper values represent extreme assumptions on the role of collisional excitation and ionisation by neutral hydrogen for the NLTE level populations of neutral oxygen. The error of our analysis is $\pm$ (0.04$\pm$ 0.03) dex, the last being related to NLTE corrections, the first error to any other effect. The 3D "granulation effects" do not play a decisive role in lowering the oxygen abundance.
Conclusions. Our recommended value is $\log(N_{\rm O}/N_{\rm H}) = 8.76 \pm 0.07$, considering our present ignorance of the role of collisions with hydrogen atoms on the NLTE level populations of oxygen. The reasons for lower O abundances in the past are identified as (1) the lower equivalent widths adopted and (2) the choice of neglecting collisions with hydrogen atoms in the statistical equilibrium calculations for oxygen.

Key words. Sun: abundances – Sun: photosphere – line: formation – hydrodynamics – convection – radiative transfer

1. Introduction

Oxygen is the most abundant element after hydrogen and helium and is the main product of type II supernovae. In the studies of chemical abundances in stars and in interstellar and intergalactic matter, it is common to use the solar or solar system abundances as a reference. Unlike many other elements, oxygen is volatile and is therefore incompletely condensed in meteorites, where it is present in the form of oxides. As a consequence, the only available reference is the solar *photospheric* oxygen abundance.

In spite of its high cosmic abundance, there are not many atomic oxygen lines that are suitable for spectroscopic abundance determinations. Oxygen in the solar photosphere is mainly present in the neutral state. The permitted resonance and low-excitation energy lines lie in the vacuum ultraviolet, many at wavelength shortward of the Lyman break. High-resolution spectra of the Sun at these wavelengths are not available. However, even if they were available, the line blending and heavy saturation of most of these lines would make them unsuitable for abundance measurements. In the optical or near infrared range, there are only a few O I lines that can be used; however, all the permitted lines are of high excitation and many of these are blended. There are three forbidden lines that arise from the ground state or very low lying levels, which, however, are very weak, and they are all more or less blended with other atomic or molecular lines. This makes the determination of the solar oxygen abundance a rather complex matter that requires special care.

Because of its high cosmic abundance, oxygen is one of the major contributors to the internal opacity of matter at solar-like chemical composition. It also plays a special role, together with nitrogen and carbon, in the energy production in the Sun. This implies that the solar oxygen abundance has a direct impact on the internal structure and evolutionary behaviour of the Sun. A solar model with reduced abundance of CNO elements has lower central density and opacity (Watson & Guzik 2006) and thus evolves more slowly than a model with higher abundances. In

⋆ This paper is dedicated to the memory of Hartmut Holweger.

the late evolution of the Sun, the CNO cycle becomes the main source of energy, and a reduced abundance of these elements, together with the lower central densities, implies a higher central burning temperature for the Sun.

The oscillatory properties of the Sun are strongly dependent on the metal content. In fact, the use of helioseismic data has been suggested for deriving Z (Antia & Basu 2006).

The solar oxygen abundance has undergone several major downward revisions over the years, starting from the value of Lambert (1978), $A(\mathrm{O}) = 8.92$[1]. The influential review of Anders & Grevesse (1989) still provided a value near this measurement ($A(\mathrm{O}) = 8.93 \pm 0.035$), but nine years later it underwent a downward update by 0.1 dex (Grevesse & Sauval 1998), then was subject to another downward revision by almost 0.1 dex due to Holweger (2001), another downward revision by Allende Prieto et al. (2001), and finally was lowered again down to the extremely low value of $A(\mathrm{O}) = 8.66$ recommended by Asplund et al. (2004). The last result is supported by Meléndez (2004) and Socas-Navarro & Norton (2007). However, the recent result of Ayres et al. (2006, $A(\mathrm{O}) = 8.84$), based on CO infrared lines, is a countertrend.

The very low abundance advocated by Asplund et al. (2004), together with the downward revision of the solar abundances of all the other elements by Asplund and collaborators (Asplund et al. 2005, and references therein), has created serious problems for solar models to explain the helioseismic data (Bahcall et al. 2005a,b; Guzik et al. 2006).

So far, the only three analyses of the solar oxygen abundance that take the effects of photospheric inhomogeneities (granulation effects) into account are those of Holweger (2001), Allende Prieto et al. (2001), and Asplund et al. (2004). The recommended oxygen abundances differ by almost 0.1 dex. According to our analysis based on 3D CO^{5}BOLD solar models, the granulation effects do not lead to a systematic lowering of the oxygen abundance. The 3D corrections we find are small and, for the majority of the lines, positive.

We present here a new and independent determination of the solar oxygen abundance, with particular emphasis on a latest generation 3D CO^{5}BOLD[2] solar model, which, we believe, helps in understanding possible underlying systematic errors in the modelling of the solar photosphere. The line-by-line analysis is presented with full details in the next sections. However, the paper is organised in such a way that the reader not interested in such details may skip directly to the discussion and conclusions in Sect. 6.

2. Atomic data

The atomic data on oxygen lines is reviewed in detail in Sect. 2.1 of Asplund et al. (2004, hereafter A04). For the lines in common we adopt the same data, and we refer the reader to that paper for further details. In addition to the atomic lines used by A04 we make use of two IR lines: the 1316 nm line, for which we adopt the log gf of Biémont et al. (1991), and the 1130 nm line, for which we use the NIST value of log $gf = 0.076$, the same value used by Holweger (2001). The adopted atomic data are summarised in Table 1.

For the collisional broadening constants $\log(\gamma_6/N_\mathrm{H})$ given in Table 1, we paid particular attention in our 3D spectrum synthesis computations to the Van der Waals broadening of the oxygen lines to obtain as realistic line profiles as possible. While this broadening process is important for the *strength* of strong lines it also plays a role for the *shape* of weak lines. From that perspective we deemed appropriate to provide the actual values that we employed. Whenever available we preferred Van der Waals broadening constants obtained from the theory of Anstee & O'Mara (1995), Barklem & O'Mara (1997), Barklem et al. (1998a), and summarised in Barklem et al. (1998b). Hereafter, we collectively refer to the description as the "ABO theory". ABO theory predicts a slightly different temperature dependence of the broadening effects than does classical theory. It is customary to give the broadening constants for a Maxwellian (relative) velocity distribution at 10^4 K. We did not implement the ABO theory in our 3D spectrum synthesis code, but instead opted to ignore the slight differences in the temperature dependences and to choose a reference temperature of 5500 K at which we evaluated the broadening constants from ABO theory. This ensures that our classical implementation provided the ABO value at this temperature. The reference temperature was chosen as characteristic of the lower photospheric layers of the Sun. This is the reason we give the broadening constants in a non-standard fashion with reference to 5500 K in Table 1.

Alternatively, we computed Van der Waals broadening constants from the approximation implemented in the Kurucz routine WIDTH (see Ryan 1998). In short, the WIDTH approximation is the following: $C_6 = (\alpha e^2)/h\,(45 - S)/Z$, where S is the number of electrons in the ion under consideration and Z is the nuclear charge (for neutral oxygen $S = 8$ and $Z = 8$). Then $\gamma_6/N_\mathrm{H} = 17 C_6^{2/5} v^{3/5}$, where v is the average relative velocity of the atom with respect to the perturber (Gray 2005, Eq. (11.28)). The results are listed in Table 1.

Table 1. Atomic parameters of the oxygen lines included in our analysis.

Wavelength in air [nm]	Trans.	log gf	χ_lo [eV]	log (γ_6/N_H) @ 5500 K [s^{-1} cm^3]	
				ABO	WA
630.0304	^{3}P–^{1}D	–9.717	0.000		–8.362
636.3776	^{3}P–^{1}D	–10.185	0.020		–8.364
615.81	^{5}P–^{5}D	–0.296	10.741	–6.948	–7.246
777.1941	^{5}S–^{5}P	0.369	9.146	–7.569	–7.741
777.4161	^{5}S–^{5}P	0.223	9.146	–7.569	–7.741
777.5390	^{5}S–^{5}P	0.001	9.146	–7.569	–7.741
844.6759	^{3}S–^{3}P	0.014	9.521	–7.511	–7.709
926.66	^{5}P–^{5}D	0.825	10.741	–7.334	–7.489
1130.2377	^{5}P–^{5}S	0.076	10.741	–7.141	–7.565
1316.4	^{3}P–^{3}S	–0.033	10.99	–7.108	–7.555

"ABO" refers to results from ABO theory, "WA" to the WIDTH approximation (see text for details).

3. Codes and atmospheric models

Our analysis is based on a time-dependent 3D hydrodynamical model of the solar photosphere, as well as on a number of standard 1D hydrostatic models. The 3D model was computed with the CO^{5}BOLD code (Freytag et al. 2002, 2003; Wedemeyer et al. 2004). An overview of the numerics, aspects of the methodology of its application, and basic validity tests can be found in Ludwig et al. (2008).

The 3D model used has a box size of $5.6 \times 5.6 \times 2.27$ Mm^3 and a resolution of $140 \times 140 \times 150$ grid points, and it spans a range in optical depth of about $-6.7 < \log \tau_\mathrm{Ross} < 5.5$. The multi-group opacities used by CO^{5}BOLD are based on

[1] $A(\mathrm{X}) \equiv \log(N_\mathrm{X}/N_\mathrm{H}) + 12$.

[2] http://www.astro.uu.se/~bf/cobold/index.html

monochromatic opacities stemming from the MARCS stellar atmosphere package (Gustafsson et al. 2007, 2003) provided as a function of gas pressure and temperature with high wavelength resolution. For the calculation of the opacities, solar elemental abundances according to Grevesse & Sauval (1998) are assumed, with the exception of CNO for which values close to the recommendation of Asplund et al. (2005) are adopted (specifically, A(C) = 8.41, A(N) = 7.80, A(O) = 8.67). The monochromatic opacities are binned into representative opacity groups (Nordlund 1982; Ludwig 1992; Ludwig et al. 1994; Vögler 2004). The solar CO^{5}BOLD model applied here uses twelve bins; to our knowledge, this is the highest wavelength resolution hitherto applied in a 3D stellar atmosphere model.

The equation of state takes the ionisation of hydrogen and helium into consideration, as well as the formation of H_2 molecules according to Saha-Boltzmann statistics. It ignores the ionisation of the metals, which is of minor importance (<1 %) for the bulk thermodynamic properties. Relevant thermodynamic quantities – in particular gas pressure and temperature – are tabulated as a function of gas density and internal energy. To ensure accuracy in higher derivatives (like the adiabatic sound speed) analytical first derivatives are tabulated as well.

The tabulated EOS is only used for the computation of the bulk thermodynamic quantities (like gas pressure, temperature, sound speed, specific heats) needed in the hydrodynamical simulations. The electron pressure is not relevant in this context. In contrast, for the post facto spectrum synthesis from selected snapshots, a precise calculation of the electron pressure is important. A more detailed LTE EOS, including the formation of H^- and the multiple ionisation of all individual metals, is employed for this purpose.

We emphasise that our finally obtained oxygen abundance is not used to alter the 3D model atmosphere consistently. Besides the substantial computational efforts, we believe that the feedback would be very small, in particular since oxygen is not a significant electron contributor. We tested the feedback in the spectral synthesis: changing the oxygen abundance by 0.1 dex or changing the oscillator strength by 0.1 dex gave line strengths of the 630 nm forbidden oxygen line differing by only 0.1%.

For statistically representing the solar atmosphere, we selected 19 snapshots equidistantly spaced in time covering in total 1.2 h of solar time. The snapshots are separated in time enough so that their flow patterns are largely uncorrelated. They have been further selected to have statistical properties close to the properties of the whole ensemble of available snapshots. We restricted ourselves to a subset of the available 3D data to keep the computational burden manageable. Here, in Fig. 1, we only show a comparison of the average CO^{5}BOLD model with the 3D model used by A04 in their re-determination of the solar oxygen abundance. The CO^{5}BOLD model was averaged on surfaces of equal Rosseland optical depth. The Rosseland scale was subsequently transformed to an optical depth scale at 500 nm in the continuum to allow a direct comparison to the model published by A04. This is not exactly identical to an averaging on $\tau_{500\,\mathrm{nm}}$ surfaces as done by A04, but we consider the involved inconsistencies immaterial for the present discussion. For further comparison and a benchmark, we added the empirical Holweger-Müller solar model (Holweger 1967; Holweger & Müller 1974, hereafter HM) to the plot. In the low photospheric layers ($-0.7 < \log\tau < 0$), the average CO^{5}BOLD stratification follows the HM model rather closely. As a consequence, the CO^{5}BOLD model reproduces the observed solar centre-to-limb variation in the continuum remarkably well (see Ludwig et al. 2008). In this region the A04 model has a steeper

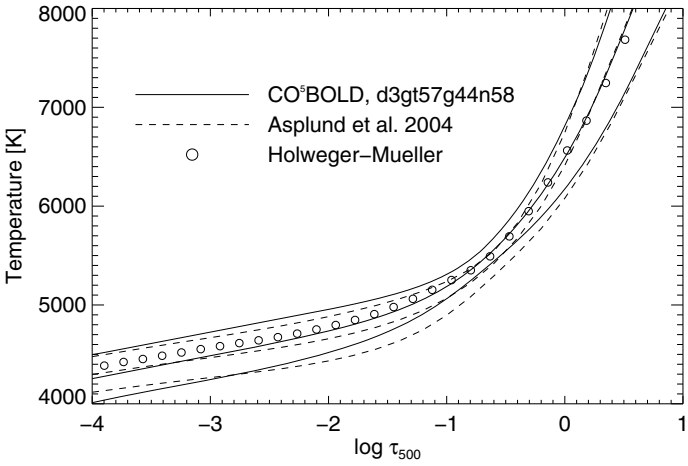

Fig. 1. Comparison of the temperature structures of the CO^{5}BOLD model used in this work, the 3D model of A04, and the Holweger-Müller model. For the 3D models the RMS fluctuations (thin lines) around the mean (thick lines) are indicated.

temperature gradient and becomes gradually cooler than the HM model. Towards lower optical depth, the CO^{5}BOLD model becomes increasingly cooler than the HM model, while the A04 model approaches the HM stratification due to the different mean temperature gradients of the models. In any case, both hydrodynamical models stay systematically cooler than the HM model. In the higher photosphere ($\log\tau < -2$), the CO^{5}BOLD model exhibits larger temperature fluctuations than the A04 model.

It is unclear which of the 3D models provides the better representation of the solar photosphere. Nonetheless, we think the differences seen in Fig. 1 provide an estimate of the systematic uncertainties that are present in the current generation of hydrodynamical model atmospheres.

As a reference we also used several 1D LTE plane parallel solar model atmospheres:

1. an ATLAS model computed by Fiorella Castelli[3] with version 9 of the ATLAS code and the solar abundances of Asplund et al. (2005). With respect to other ATLAS solar models, this has been computed with an opacity distribution function explicitly computed for the solar chemical composition of Asplund et al. (2005), a micro-turbulent velocity of 1 km s^{-1}, and a mixing-length parameter $\alpha_{\mathrm{MLT}} = 1.25$;
2. a solar MARCS model[4], also computed for a micro-turbulent velocity of 1 km s^{-1}, but with $\alpha_{\mathrm{MLT}} = 1.5$ (Gustafsson et al. 2003, 2007);
3. the Holweger-Müller semi-empirical solar model (Holweger 1967; Holweger & Müller 1974);
4. an *average* 3D model denoted by ⟨3D⟩, generated by Linfor3D[5]; this provides a 1D atmospheric structure by averaging each 3D snapshot over surfaces of equal (Rosseland) optical depth (cf. Fig. 1);
5. a 1D hydrostatic model which employs the same microphysics as CO5BOLD, but uses the mixing-length theory to treat convection (hereafter 1D$_{\mathrm{LHD}}$, see Caffau & Ludwig 2007, for details). We fixed the mixing-length parameter to $\alpha_{\mathrm{MLT}} = 1.0$ and considered two micro-turbulence velocities,

[3] http://wwwuser.oats.inaf.it/castelli/sun/ap00t5777g44377k1asp.dat
[4] http://marcs.astro.uu.se/
[5] http://www.aip.de/~mst/Linfor3D/linfor_3D_manual.pdf

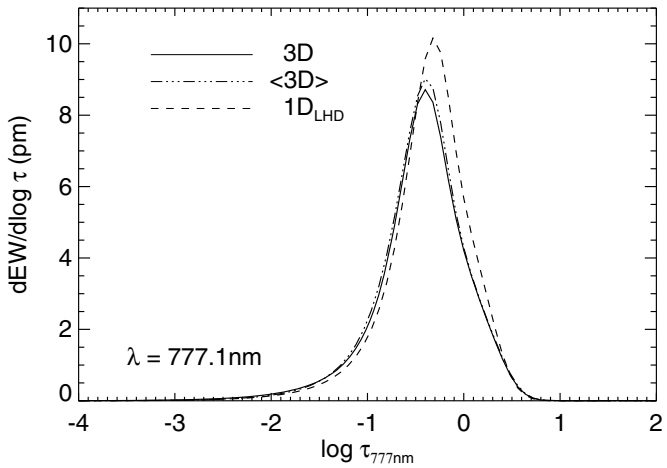

Fig. 2. The equivalent width contribution function, dEW/dlog τ, for the 777.1 nm line at disc-centre, calculated from the 3D model (solid line), the ⟨3D⟩ model (triple dot-dashed), and the 1D$_{\rm LHD}$ model (dashed). Following Magain (1986), the contribution function is defined such that integration over log τ_λ gives the line equivalent width.

1.0 and 1.5 km s^{-1}. We use this model as a reference for differential 1D–3D comparison.

The spectrum synthesis on the 3D models is done with Linfor3D. A detailed LTE equation of state was employed to provide the electron pressure and the number density of all individual atoms and ions. One limitation of the current version of Linfor3D is that it cannot handle a large number of lines; furthermore, even if it could, the computational effort would be prohibitive. We used Linfor3D to compute 3D, as well as 1D, synthetic spectra, for direct comparison to the hydro-model. For the 1D synthesis we also used SYNTHE (Kurucz 1993b, 2005b) in its Linux version (Sbordone et al. 2004; Sbordone 2005), which has no limitation in the number of lines and therefore allows including a large number (∼1000 for a range of 1 nm) of atomic and molecular lines to take the blending of very weak lines into account in great detail. In addition, we employed WIDTH (Kurucz 1993a, 2005b; Castelli 2005; Sbordone 2005) to derive 1D abundances directly from measured equivalent widths.

The global effect produced by many weak lines is similar to that of an additional continuous opacity. In principle it is possible to do an appropriate "re-normalisation" of the spectrum and compare this to a synthetic spectrum computed without including these very weak lines. We tested this procedure with 1D synthetic spectra and found it to be acceptable, at least as a first approximation, introducing errors in the derived abundance of less than 0.01 dex. Therefore our approach has been to use this technique for the 3D analysis, keeping only a minimal number of lines ($n < 10$) in the computation.

Departures from LTE are non-negligible for several permitted O I lines, most noticeably for the 777 nm triplet. At present our 3D-NLTE line formation code by Steffen & Cayrel (see Cayrel et al. 2007) is not capable of treating oxygen, and we defer full 3D-NLTE computations to a future paper. However, in the case of O I lines, 1D computations should yield a reliable estimate of departures from LTE. In fact the line formation range in the solar photosphere is very similar in 3D and 1D$_{\rm LHD}$ models, respectively, for the oxygen triplet (see Fig. 2), and also for the other infrared oxygen lines. This is not necessarily valid for other elements and other stellar models. For instance, 3D-NLTE and 1D-NLTE contribution functions of the

Table 2. Ni I isotopic splitting.

Ni I isotope	%	Wavelength	log gf	% used
^{58}Ni I	68.27	630.0335	–2.11	72.34
^{60}Ni I	26.10	630.0355	–2.11	27.66
^{58}Ni I	68.27	630.0335	–2.11	69.05
^{60}Ni I	26.10	630.0355	–2.11	26.40
^{62}Ni I	3.59	630.0375	–2.11	3.63
^{64}Ni I	0.91	630.0395	–2.11	0.92

670.8 nm ^{7}Li line are very different for a metal-poor model at $T_{\rm eff} = 6240$ K, log $g = 4.0$, [M/H] = –2.0 (Cayrel et al. 2007). Even if the *mean* vertical stratification of oxygen is very similar in 1D and 3D, horizontal inhomogeneities could introduce a difference between 1D and 3D NLTE corrections. The error due to the 1D approximation needs to be quantified by future detailed 3D-NLTE calculations.

The similarity between NLTE corrections computed in 1D and 3D is confirmed by the results in Table 2 of A04. We suspect that the two corrections would have been even closer if the authors had used a model with the mean temperature structure of their 3D model as a background model for their 1D-NLTE computations.

For the present paper we decided to compute 1D-NLTE corrections based on the ⟨3D⟩ model (rather than on 1D$_{\rm LHD}$) and to use the Kiel code (Steenbock & Holweger 1984), together with the oxygen model atom described in Paunzen et al. (1999). We also compared our NLTE corrections with those computed by Holweger (2001) and A04.

4. Observational data

There are several high-resolution, high signal-to-noise ratio (S/N) spectra both of the solar flux and of the disc-centre intensity, and we decided to make use of all of them. The choice of using more than one solar atlas stems the fact that, even if S/N is very high for solar spectra, the abundances obtained from different spectra do not always agree within one σ, highlighting the existence of systematic differences, which are not fully understood.

1. the data we refer to as "Kurucz flux" spectrum is based on fifty solar FTS scans taken by James Brault and Larry Testerman at Kitt Peak between 1981 and 1984, with a spectral resolving power $\lambda/\Delta\lambda$ of the order of 300 000 and an S/N of around 3000, both varying from range to range. Further details can be found in Kurucz (2005a);
2. the "Neckel flux" and "Neckel intensity" spectra refer to the Neckel & Labs (1984) absolutely calibrated FTS spectra obtained at Kitt Peak in the 1980s, covering the range 330 nm to 1250 nm for full-disc and disc-centre, respectively (see also Neckel 1999). The spectral purity ($\Delta\lambda$) ranges from 0.4 pm at 330 nm to 2 pm at 1250 nm (825 000 > $\lambda/\Delta\lambda$ > 625 000) ;
3. Delbouille et al. (1973) provide a disc-centre intensity spectrum in the range 300 nm to 1000 nm observed from the Jungfraujoch[6]. At the same web site, an infrared disc-centre intensity spectrum, observed from Kitt Peak by Delbouille et al. (1981), is also available; this spectrum covers the range from 1000 nm to 5400 nm. In the following we refer to both atlases, for brevity, as the "Delbouille intensity";

[6] http://bass2000.obspm.fr/solar_spect.php

4. Wallace et al. (1996) present disc-centre intensity FTS spectra obtained at Kitt Peak by Pierce (1964). We refer to this data as the "Wallace Intensity";
5. for the infrared lines at 1130 nm and 1316 nm, we analysed Kitt Peak FTS spectra from the Digital Archive of the National Solar Observatory as reduced by one of the authors (TRA).

The light emerging from the Sun is subject to a gravitational redshift of 636 m s^{-1}; of the atlases we employ, only the Kurucz flux has been corrected for this effect. In addition, one should take the effect of the Earth's rotation into account at the time the spectrum was acquired. Again only the Kurucz flux has been carefully corrected for this effect. In principle the wavelength precision of the FTS scans is extremely high; that is, wavelengths measured at one end of the scan are very close relative to wavelengths measured at the other end of the scan. In the terrestrial reference frame, the scans are highly accurate, since they are slaved to a laser. However, the absolute accuracy depends on how well one has corrected for all the other effects. Then there is the additional issue of how well the laboratory wavelengths of the oxygen lines themselves are known. Considering in addition that the convective line shifts predicted by our hydrodynamical simulations are not perfectly accurate (we estimate the accuracy to be of the order of 50 m s^{-1}), we decided to introduce the wavelength shift between observed and synthetic spectrum as free parameter in the spectral line fitting procedure described below.

Considering the six oxygen lines at 630, 636, 777 and 844 nm, we measure the following wavelength shifts, with respect to the laboratory wavelengths: for the Kurucz flux 21 ± 264 m s^{-1}, for the Neckel flux 388 ± 258 m s^{-1} and for the Delbouille intensity 344 ± 273 m s^{-1}. Our results are in good agreement with the Allende Prieto & Garcia Lopez (1998) data that present a σ of 238 m s^{-1} with an average of 286 m s^{-1} for iron lines in the Neckel flux spectrum.

It is not the purpose of the present paper to investigate the convective shifts of oxygen lines. What we did want to do was point out the systematic differences in absolute wavelengths between the various solar atlases. This makes it mandatory to leave the wavelength shift as a free parameter when performing line-profile fitting.

5. Data analysis

To derive oxygen abundances, we measured the equivalent width (EW) of the oxygen lines and, when possible, fitted the line profile. EWs were computed by direct numerical (trapezoidal) integration or by integration of a fitted Gaussian or Voigt profile, using the IRAF task `splot`. The results are summarised in Table 3.

All line profile fitting was performed through χ^2 minimisation using the code described in Caffau et al. (2005). Besides the oxygen abundance, the level of the continuum and a wavelength shift were also left as free parameters in the fitting procedure. For 1D models, the macro turbulence has to be fixed a priori. The whole line profile or only a selected range can be fitted, as was done, for example, for the 926 nm line because of the presence of a residual of a telluric line in one of the wings.

A change in the Van der Waals broadening constant γ_6, input to the line formation code, can produce lines with different shapes (more or less broadened) but also of different EW. For instance if we change the $\log\gamma_6$ of the 636 nm [OI] line from the standard input value for Linfor3D −8.145 to the value of −8.364 provided by the WIDTH approximation (Ryan 1998), the difference in EW is 0.2%. Considering the oxygen triplet, the EW increases by 4% to 5% (depending on the oxygen abundance) if we change the $\log\gamma_6$ from −7.57 as derived from ABO theory to −7.74 as obtained from the WIDTH approximation. We adopted the following strategy. For the transitions for which the broadening data were available from ABO we computed the $\log\gamma_6$ according to the ABO theory; when not available, we used the WIDTH approximation that is the one also used inside the SYNTHE code. We point out that, contrary to naive expectations, the broadening effect is not completely negligible for weak lines, as also pointed out by Ryan (1998). In the 615 nm line, for instance, a change in $\log\gamma_6$ of 0.16 dex, from −7.164 to −7.004, produces, for an oxygen abundance of 8.66, a difference in EW of 1%. In contrast, the [OI] lines are insensitive to the value adopted for $\log\gamma_6$.

Concerning the quadratic Stark broadening, even strong lines, such as the oxygen triplet lines, are not very sensitive to the parameter γ_4. In fact a change by a factor 2 in γ_4 produces a change in the strongest line of the triplet of $^{-0.01}_{+0.006}$ dex in the oxygen abundance according to WIDTH combined with the ATLAS model. Even the shape of the line is affected by this change very little, only the wings being appreciably different in the synthetic spectra.

Since the emphasis of this work is on the 3D analysis, we analysed all the observed spectra with CO^{5}BOLD+Linfor3D. For comparison we considered the 1D computations for EWs for all the observed spectra, but we mostly limited the 1D line-profile fitting to the Kurucz flux, when available, or to the Delbouille intensity.

As in Caffau & Ludwig (2007), we defined the "3D corrections" as the difference $A(\mathrm{O})_{\mathrm{3D}} - A(\mathrm{O})_{\mathrm{1D_{LHD}}}$, because the 3D effect is best captured when comparing the 3D and the 1D$_{\mathrm{LHD}}$ models (which share the same input physics) and using the same line formation code, Linfor3D. The resulting "3D corrections" depend on the choice of both the mixing-length parameter, α_{MLT}, and the micro-turbulence parameter, ξ, necessary for defining the 1D model. The micro-turbulence is only important for the stronger lines, in our case the triplet lines. In this study we considered two values of the micro-turbulence, $\xi = 1.0$ and 1.5 km s^{-1} (see Table 3). Apart from the triplet lines, the difference in abundance when considering the two ξ is at most 0.02 dex. For the triplet, a different choice in ξ is translated into a change in the 1D abundance by up to 0.04 dex. Higher micro-turbulence produces stronger lines in synthetic spectra, so that the oxygen abundance obtained is lower. In the present work we gave preference to $\xi = 1.0$ km s^{-1}. Concerning the 1D$_{\mathrm{LHD}}$ model for the mixing-length parameter, we took $\alpha_{\mathrm{MLT}} = 1$. Most of the lines are formed in layers that are not strongly affected by convection, hence by the choice of the mixing-length parameter. However, this is not true for the 615 nm line, which is formed in deep photospheric layers. For testing this aspect, we considered three representative lines: the strongest line of the triplet at 777.1 nm, the stronger forbidden line at 630 nm, and the line at 615 nm. We changed the mixing-length parameter by $^{+1.0}_{-0.5}$ with respect to our preferred value of 1.0. With this change in α_{MLT}, the change in the 1D$_{\mathrm{LHD}}$ oxygen abundance (for fixed equivalent width in the synthetic flux spectra) for the forbidden and the triplet line is small $^{-0.003}_{+0.011}$ for the forbidden line and $^{-0.003}_{+0.018}$ for the triplet line. In contrast, we find a change in abundance of $^{-0.045}_{+0.080}$ for the 615 nm line. This clearly indicates that, for some lines, the 3D–1D corrections depend on the mixing-length parameter assumed in the 1D comparison model.

For completeness, we also provide differences using other 1D models, either with Linfor3D or with SYNTHE. We point out, however, that these differences also depend on code specific

Table 3. Solar LTE oxygen abundance for individual lines as derived from different spectra and model atmospheres.

Spectrum	Wavelength	EW	A(O)							3Dcor			
			3D	⟨3D⟩		1D$_{\rm LHD}$		HM		3D–⟨3D⟩		3D–1D$_{\rm LHD}$	
	nm	pm		1.0	1.5	1.0	1.5	1.0	1.5	1.0	1.5	1.0	1.5
(1)	(2)	(3)	(4)	(5)	(6)	(7)	(8)	(9)	(10)	(11)	(12)	(13)	(14)
KF	615.8	0.364	8.639	8.719	8.717	8.668	8.665	8.782	8.779	–0.080	–0.077	–0.029	–0.026
NF	615.8	0.365	8.641	8.721	8.718	8.669	8.667	8.783	8.781	–0.080	–0.077	–0.028	–0.026
NI	615.8	0.539	8.645	8.705	8.701	8.666	8.663	8.785	8.782	–0.059	–0.056	–0.021	–0.018
DI	615.8	0.499	8.606	8.666	8.663	8.628	8.626	8.747	8.745	–0.060	–0.057	–0.022	–0.020
KF	630.0	0.551[1]	8.695	8.690	8.687	8.645	8.642	8.715	8.712	0.005	0.008	0.050	0.053
NF	630.0	0.530[1]	8.668	8.663	8.661	8.615	8.613	8.688	8.686	0.005	0.007	0.053	0.055
NI	630.0	0.470[1]	8.686	8.667	8.665	8.613	8.611	8.698	8.696	0.019	0.021	0.073	0.075
DI	630.0	0.457[1]	8.666	8.646	8.644	8.591	8.589	8.678	8.677	0.020	0.022	0.075	0.077
KF	636.4	0.146	8.780	8.772	8.772	8.756	8.756	8.786	8.786	0.008	0.008	0.024	0.024
NF	636.4	0.153	8.801	8.793	8.793	8.777	8.777	8.807	8.806	0.008	0.008	0.024	0.024
NI	636.4	0.139	8.837	8.822	8.822	8.802	8.802	8.839	8.839	0.015	0.015	0.035	0.035
DI	636.4	0.106	8.718	8.703	8.703	8.683	8.683	8.721	8.720	0.015	0.015	0.035	0.035
KF	777.1	8.140	9.034	9.025	8.984	8.974	8.935	9.030	8.988	0.009	0.050	0.059	0.099
NF	777.1	8.080	9.026	9.017	8.976	8.966	8.927	9.022	8.980	0.009	0.050	0.059	0.099
NI	777.1	9.290	8.952	8.912	8.870	8.841	8.802	8.934	8.892	0.040	0.081	0.111	0.150
DI	777.1	8.900	8.903	8.863	8.824	8.794	8.755	8.886	8.846	0.040	0.080	0.110	0.149
KF	777.4	6.870	8.992	8.987	8.948	8.939	8.902	8.992	8.953	0.005	0.044	0.053	0.091
NF	777.4	6.800	8.981	8.976	8.937	8.928	8.891	8.981	8.942	0.005	0.044	0.053	0.090
NI	777.4	7.870	8.912	8.875	8.836	8.807	8.770	8.899	8.860	0.037	0.076	0.105	0.142
DI	777.4	7.350	8.838	8.802	8.765	8.735	8.698	8.827	8.791	0.035	0.074	0.103	0.140
KF	777.5	5.420	8.967	8.967	8.932	8.922	8.889	8.974	8.940	0.000	0.035	0.045	0.078
NF	777.5	5.340	8.953	8.953	8.918	8.908	8.875	8.960	8.926	0.000	0.034	0.045	0.078
NI	777.5	6.280	8.895	8.863	8.829	8.800	8.766	8.891	8.857	0.032	0.066	0.095	0.129
DI	777.5	6.090	8.864	8.833	8.800	8.769	8.737	8.861	8.830	0.030	0.065	0.094	0.127
KF	844.6	3.511	8.830	8.848	8.823	8.803	8.779	8.864	8.841	–0.017	0.007	0.027	0.051
NF	844.6	3.533	8.836	8.853	8.828	8.808	8.784	8.869	8.846	–0.017	0.007	0.028	0.052
NI	844.6	4.372	8.789	8.777	8.752	8.716	8.692	8.820	8.796	0.011	0.037	0.072	0.096
DI	844.6	4.492	8.813	8.801	8.775	8.739	8.715	8.842	8.818	0.012	0.038	0.074	0.098
WI	926.6	3.829	8.736	8.744	8.731	8.677	8.664	8.799	8.787	–0.008	0.005	0.060	0.072
AI	1130.2	1.920	8.748	8.759	8.752	8.706	8.700	8.824	8.818	–0.011	–0.004	0.042	0.048
AI	1316.5	1.980[2]	8.767	8.767	8.762	8.740	8.735	8.835	8.830	0.000	0.005	0.027	0.031
AI	1316.5	3.150[3]	8.763	8.766	8.763	8.741	8.739	8.833	8.830	–0.003	0.000	0.022	0.024

Column (1): spectrum identification: DI: Delbouille intensity, NI: Neckel intensity, WI: Wallace intensity, AI: Ayres intensity, NF: Neckel flux, KF: Kurucz flux. Column (2): wavelength of the line. Column (3): measured equivalent width. Column (4): oxygen abundance, A(O), according to the CO^{5}BOLD 3D model. Columns (5)–(10): A(O) from 1D models, odd numbered columns correspond to a micro-turbulence ξ of 1.0 km s^{-1}, even numbered columns to ξ = 1.5 km s^{-1}. Columns (11)–(14): 3D corrections, even numbered columns for ξ = 1.0 km s^{-1}, and odd numbered columns for 1.5 km s^{-1}, respectively.
(1) EW of the blend [O I]+Ni I; the contribution to the EWs due to Ni for A(Ni) = 6.25 is 0.20 and 0.18 pm for flux and intensity spectra, respectively, according to our 3D investigation. (2) EW relative to the two blending O I lines of the multiplet. (3) EW relative to the complete multiplet.

disparities such as different opacities, partition functions, radiative transfer schemes, etc, and thus serve mainly to illustrate the magnitude of systematic modelling uncertainties.

5.1. Corrections for departure from local thermodynamic equilibrium

Besides the fact that Holweger (2001) computed 1D-non-LTE and A04 3D-non-LTE, the differences in the two NLTE computations is the way in which excitation and ionisation by inelastic collisions with hydrogen atoms is accounted for. Holweger (2001) accounts for them by using the formalism of Steenbock & Holweger (1984), which is a generalisation of the one in Drawin (1969). A04 instead totally ignore them.

The two reasons favouring ignoring collisions with hydrogen atoms are (i) the larger cross-section for collisions with electrons and (ii) the fact that electrons have much higher velocities, thereby making collisions with e$^-$ far more frequent. On the other hand, the ratio of hydrogen atoms to electrons is often as high as 10^4 or even 10^5. Under these circumstances, it appears difficult to deny the role of collisions with hydrogen atoms.

In our solar model, $N_{\rm H}/N_{\rm e}$ is almost flat at 10^4 in the outer layers, it is about 0.8×10^4 at $\log \tau_{\rm Ross} = -0.5$ and then drops dramatically to ∼70 at $\log \tau_{\rm R} = 1$. One should therefore expect that the role of collisions with hydrogen atoms is different for lines having different line formation depths.

Since the Steenbock & Holweger (1984) formalism is the only practical way to include the effects of collisions with

hydrogen atoms, it has become customary in NLTE codes to adopt it and to introduce the scaling factor $S_{\rm H}$. A zero value for this scaling factor is equivalent to ignoring the process. For some species, like Na and Li, for which laboratory data exist, it is known that the classical Drawin formula (Drawin 1969) leads to overestimating the collisional rates (see Asplund et al. 2004, and references therein). Unfortunately, no laboratory data exists for collisions of neutral hydrogen with oxygen. Inspection of the literature shows that very different choices for $S_{\rm H}$ are made for different species. For example Gehren et al. (2001) advocate $S_{\rm H} = 5$ for Fe I in the Sun.

Allende Prieto et al. (2004) have used the centre-to-limb variations of the 777 nm O I triplet to constrain the role of collisions with hydrogen atoms. Their χ^2 analysis of synthetic NLTE profiles computed from their 3D hydrodynamical simulation favours $S_{\rm H} = 1$. In several papers the Kiel group has adopted $S_{\rm H} = 1/3$ (Solanki & Steenbock 1988; Stürenburg & Holweger 1990, 1991), mainly based on the unpublished work of Steenbock. In the present paper we present NLTE corrections for $S_{\rm H} = 0, 1/3, 1$ and discuss the implications.

5.2. Error estimates

We here consider the possible errors that affect the analysis of the oxygen abundance in each line. We will take the following errors into account for each line: "log gf error", "broadening theory error", "blending error", "NLTE correction error", "statistical error".

1. The "log gf error": the uncertainty of log gf translates directly into an error of the oxygen abundance. Since Storey & Zeippen (2000) do not report an error estimate of log gf for the two forbidden lines, we considered as the error in log gf the difference between the value given by Storey & Zeippen (2000) and the value used by Lambert (1978), which has been widely used prior to the Storey & Zeippen (2000) computations. For the other oxygen lines, we used the error of the f-value as listed in the NIST Atomic Spectra Database[7].
2. The "broadening theory error": in our analysis we applied, whenever possible, the ABO broadening theory. However, for some lines the use of the WIDTH approximation would result in a different abundance. We therefore consider the difference in the derived abundance using the two different broadening theories as an upper limit of the uncertainty associated with the broadening theory itself.
3. The "blending error": some oxygen lines are blended with other lines, either stellar or telluric. Uncertainties in the atomic data of the blending line(s), as well as uncertainties in the abundances of the involved species, introduce additional errors that propagate to the final oxygen abundance. In some cases, the presence of a neighbouring line, influencing the wings of the oxygen line in question, can produce an uncertainty in the placement of the continuum. This is the case, e.g., for the 844 nm line. These two kinds of uncertainties associated with blending were considered together. The error due to uncertain continuum placement, which itself is caused by blends in the line wings, has been estimated through successive trials, identifying the "highest acceptable" and "lowest acceptable" continuum level. There is clearly some degree of subjectivity in this estimate. However, we were unable to devise a more objective approach. An uncertainty is introduced when the telluric absorption is subtracted from the spectrum.
4. The "NLTE correction error": the choice on the value to assign to the H-atom collision scaling factor, $S_{\rm H}$, changes the NLTE correction. As the related uncertainty we use the difference in the (logarithmic) NLTE abundance correction between $S = 0$ and $S = 1/3$.
5. The "statistical error": is simply the standard deviation of the abundances derived from the different observed spectra.

The error related to the S/N, estimated from the Cayrel formula (Cayrel 1988), is completely negligible in comparison to the errors listed above. The differences between different solar atlases cannot be due to the random noise in the spectra, which is very low for all the data considered here, but must be related to some undetected systematic effects.

The uncertainties are summarised in Table 4. The column "total error" of this table considers the global uncertainty that we attribute to each line. This value is the quadratic sum of all the uncertainties. The error related to the NLTE computations is not included in Table 4 because it is considered as a systematic error. Details of the derived NLTE corrections are instead listed in Table 5.

5.3. Detailed analysis of individual transitions

In this section we give the details of the analysis of each of the considered transitions. The results are summarised in Tables 3 and 4. Initially, we also considered the 557 nm forbidden line, but discarded it because both the Delbouille intensity and the Kurucz flux show an asymmetry in the line profile, caused by the presence of C_2 lines, as pointed out by Lambert (1978). Unfortunately the molecular data for these C_2 lines is still not of sufficient quality to allow a reliable synthesis of the profile.

5.3.1. [O I] 630 nm

This weak line (see Fig. 3) arises from the ground level and is immune to departures from LTE, so it has always been considered a primary indicator of the photospheric oxygen abundance. However, it is blended with an Ni I line and lies next to two stronger lines[8], whose wings can influence the EW of the oxygen line if not taken into account properly. In Fig. 4 the contribution of nickel is compared to the blend [O I]+Ni I according to a 3D synthetic spectrum.

The blending nickel line exhibits a complex isotopic structure (see Table 2). The two main components are ^{58}Ni I and ^{60}Ni I, with an isotopic ratio of 0.38 and λ of 630.0335 nm and 630.0355 nm, respectively (see Bensby et al. 2004). Each component of the nickel blend is assumed to have log $gf = -2.11$ (Johansson et al. 2003). The two other even isotopic components, ^{62}Ni I and ^{64}Ni I, can be inserted in the line list as well, even if this does not change the line shape significantly, assuming that their shift with respect to the other even components has the same value as the shift between ^{58}Ni I and ^{60}Ni I (about 0.002 nm, see Rosberg et al. 1993). Rosberg et al. (1993) studied the isotope splitting of the even components of Ni II and showed that the splitting is equidistant for any of the even components of Ni II they studied. We assume the same behaviour for Ni I. We adopted A(Ni) = 6.25 (Grevesse & Sauval 1998) and consider it as a fixed parameter in the oxygen abundance determination.

[7] http://physics.nist.gov/PhysRefData/ASD/index.html, Ralchenko (2005).

[8] Si I line: $\lambda = 629.9599$ nm, log $gf = -1.50$, $\chi_{\rm lo} = 5.948$ eV; Fe I line: $\lambda = 630.1501$ nm, log $gf = -0.72$, $\chi_{\rm lo} = 3.654$ eV.

Table 4. Oxygen LTE abundance for each line with the error estimates.

Line nm	$A(O)_{3D}$	$A(O)_{HM}$	Statistical error	log gf error	Broadening error	Blend error	Total error	Spectrum
615.8	8.64	8.78	0.01	0.16	0.01	0.14	0.21	F
615.8	8.63	8.77	0.02	0.16	0.01	0.14	0.21	I
630.0	8.68	8.69	0.02	0.03	0.00	0.15	0.15	F/I
636.3	8.78	8.79	0.05	0.03	0.00	0.12	0.12	F/I
777.1	9.03	9.03	0.00	0.07	0.06	0.08	0.12	F
777.1	8.93	8.91	0.01	0.07	0.07	0.05	0.11	I
777.4	8.99	8.99	0.01	0.07	0.05	0.06	0.11	F
777.4	8.88	8.86	0.02	0.07	0.06	0.06	0.11	I
777.5	8.96	8.97	0.00	0.07	0.04	0.06	0.10	F
777.5	8.88	8.88	0.01	0.07	0.03	0.06	0.10	I
844.6	8.83	8.87	0.00	0.23	0.03	0.24	0.33	F
844.6	8.80	8.83	0.00	0.23	0.03	0.24	0.33	I
926.6	8.74	8.80	0.01	0.07	0.02	0.09	0.12	I
1130.2	8.75	8.82	0.01	0.07	0.01	0.15	0.17	I
1316.4	8.76	8.82	0.01	0.16	0.01	0.15	0.22	I

The second and third columns are the LTE abundance using the CO^{5}BOLD 3D and HM model, respectively. The last column indicates whether a flux (F) or intensity (I) measurement was used.

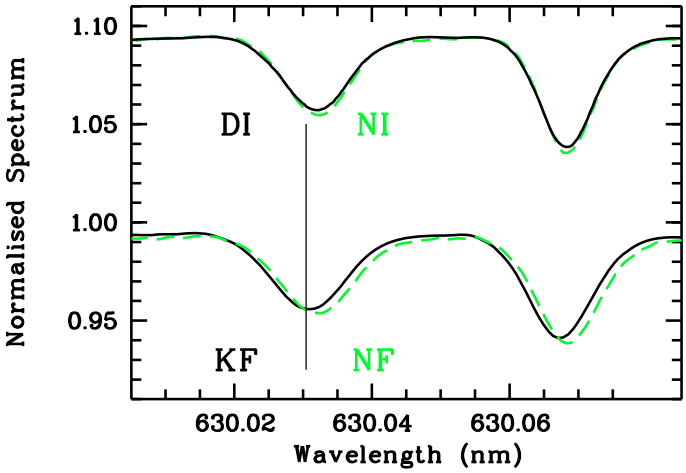

Fig. 3. The four observed spectra we used for the analysis of the [O I] 630 nm line. The Kurucz flux spectrum, KF, and the Neckel flux, NF, and Neckel intensity, NI, spectra plotted here are the normalised spectra provided by Kurucz (2005a) and Neckel (1999); the NI is shifted up by 0.1 for clarity, while the Delbouille intensity, DI, has been normalised and then shifted up by 0.1. The vertical line indicates the laboratory wavelength of the oxygen line. We recall that KF is corrected for gravitational redshift while NF is not, explaining the large wavelength differences between the two flux atlases.

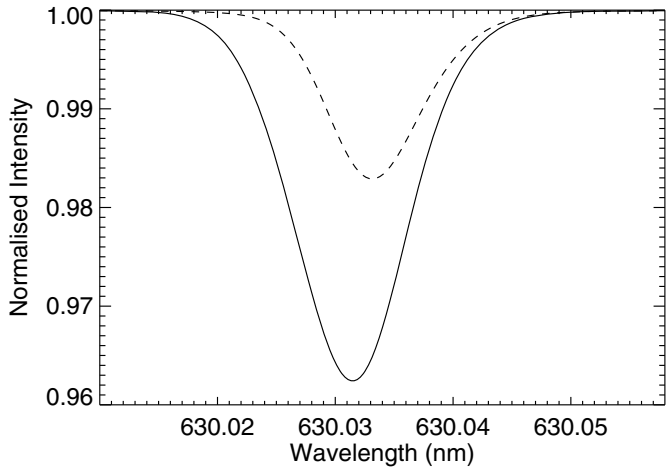

Fig. 4. The contribution of Ni I line (dashed line) with $A(Ni) = 6.25$ is compared to the combined [O I]+Ni I blend (solid line) for disc-centre according to the Linfor3D computation with $A(O) = 8.66$.

The observed solar spectra were renormalised in order to remove the silicon and iron contributions, and the *EW* of the observed spectra were computed with the program `splot`. The oxygen abundances obtained from the curve-of-growth computed with Linfor3D are reported in Table 3. Note that the abundance obtained from HM+Linfor3D is only *slightly higher* by ≈0.015 dex. On the other hand, both 1D ATLAS and MARCS models, in combination with the WIDTH line formation code, imply a *lower* oxygen abundance by 0.03 dex. In this respect both MARCS and ATLAS models behave in a similar way to the LHD model. As can be deduced from Table 3, the difference 3D–⟨3D⟩ is considerably smaller than the difference 3D–1D$_{LHD}$, meaning that the latter difference is dominated by the different mean temperature structures rather than by horizontal temperature fluctuations.

We disagree on the sign of the 3D–1D correction for this line with what was previously found by A04, whose results imply a 3D correction $A(O)_{3D} - A(O)_{1DMARCS}$ of −0.04 dex for the flux, while we find a value of +0.03 dex (see above). Our 3D correction for this line is about +0.05 dex for the flux and +0.07 dex for the intensity spectra. The influence of the micro-turbulence is completely negligible for this line.

From this line, fixing $A(Ni) = 6.25$, the 3D oxygen abundance is 8.679 ± 0.014 if we consider all four spectra. If we consider only the two flux spectra $A(O)_{3D}$ = 8.681 ± 0.019, and $A(O)_{3D}$ = 8.676 ± 0.014 from the two disc-centre spectra. *Fitting* the line profile of the solar intensity and flux spectra with a CO^{5}BOLD+Linfor3D grid of synthetic spectra, we obtain an oxygen abundance which perfectly agrees with the results from the *EW*s (Table 3) within 0.01 dex (see Fig. 5).

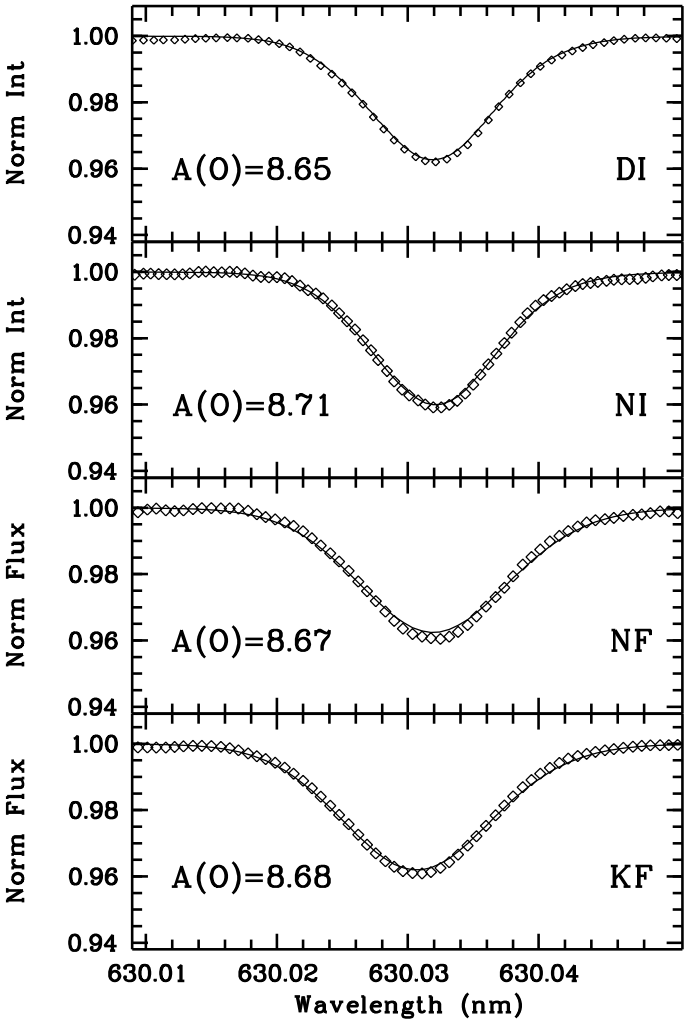

Fig. 5. The 3D fit of the [OI] 630 nm line. The observed spectra (diamonds, their size indicating the observational noise level) are superimposed on the best fit 3D synthetic line profile (solid). From top to bottom, the spectra are: Delbouille intensity (DI), Neckel intensity (NI), Neckel flux (NF), and Kurucz flux (KF).

Even if not able to reproduce the line shape satisfactorily, the 1D fits agree with the 3D results, further supporting the notion that the 3D correction is small. The line fit using SYNTHE slightly *underestimates* the oxygen abundance (HM model $A(\mathrm{O}) = 8.67$, MARCS model $A(\mathrm{O}) = 8.65$ ATLAS model $A(\mathrm{O}) = 8.61$), in agreement with the above result based on matching the *EW* with 1D models.

Since this oxygen line is blended with the neutral nickel line, a possible approach is to use a multi parameter fit, with oxygen and nickel abundance, wavelength shift, and continuum level as free parameters. We attempted this, but the result was not satisfactory because wavelength shift and nickel abundance turned out to be closely correlated parameters, thus producing a range of degenerate solutions for the best fit. However, if the wavelength scale can be established by other methods, the degeneracy is removed and both the nickel and the oxygen abundance can be found from line fitting (see Ayres 2008, and Sect. 6 below).

Since an error in the parameters of the nickel line introduces an error of the oxygen abundance, we computed two additional 3D grids where we varied the Ni I abundance by ±0.1 dex with respect to its fiducial value of 6.25. Noting that the error of the solar nickel abundance is 0.04 dex (Grevesse & Sauval 1998), and the error of the log gf value of this line is 0.06 dex (Johansson et al. 2003), a variation of ±0.1 dex in the strength of the nickel line takes the possible uncertainties into account. Our evaluation of the systematics induced in the oxygen abundance shows that a difference of ±0.1 in the nickel abundance produces a difference in the oxygen abundance of $^{-0.03}_{+0.05}$ (resulting in $A(\mathrm{O}) = 8.66, 8.74$ respectively) in the fitting of the Kurucz flux. Similar values are obtained for the Delbouille intensity (a ±0.1 change in nickel implies ∓0.06 change in oxygen abundance).

Our adopted oxygen abundance for this line comes from the average value of the four observed spectra, and it is $A(\mathrm{O}) = 8.68 \pm (0.014)_{\mathrm{stat}} \pm (0.15)_{\mathrm{syst}}$ (see Table 4 for details). The systematic error is the quadratic sum of the log gf error and the error related to blends and uncertainties in the continuum placement. The error due to the broadening theory is completely negligible for this line, being of the order of 10^{-4} dex. The final result is $A(\mathrm{O}) = 8.68 \pm 0.15$.

5.3.2. [OI] 636 nm

This line lies on the red wing of a Ca I auto-ionisation line (see Fig. 6). Several CN lines are present in the range. For C and N abundances we adopted 8.39 and 7.80, respectively. Their contribution to the *EW* of the [OI] 636 line, according to our ATLAS+SYNTHE synthesis, is 0.05 pm in flux and 0.03 pm in intensity. With a CO5BOLD+Linfor3D synthetic spectrum, the CN molecules happen to come out stronger by 20% with respect to the 1D ATLAS+SYNTHE result. This implies a difference of only 0.002 dex in the derived oxygen abundance, which is far from being able to explain the 0.1 dex difference between the oxygen abundance provided by this line (see below) and that of the 630 nm forbidden line (see Table 3).

At first we tried to remove the contribution of all the blending lines by dividing the observed spectrum by a 1D synthetic spectrum computed with all relevant atomic and molecular lines (including the Ca I auto-ionisation line) *except* oxygen. We obtained an oxygen abundance ($A(\mathrm{O}) = 8.78$), inconsistent with what was derived from the other forbidden line ($A(\mathrm{O}) = 8.68$). This is at variance with what was found by A04, according to their analysis, the difference in abundance is only 0.02 dex. This can stem from the differences in the *EW*s. But a difference of 0.06 pm in *EW* for this line can hardly explain the difference in $A(\mathrm{O})$. A difference must rely on the spectral-synthesis code used in the two analysis. Next, we normalised the spectrum following the profile of the Ca I auto-ionisation line. From the *EW* measured from this normalised spectrum, we subtracted the contribution due to CN molecules and obtained the oxygen abundances reported in Table 3. Our oxygen abundance for this line relies therefore only on the *EW* approach.

We point out that the three spectra observed from Kitt Peak (Neckel and Kurucz) imply a higher oxygen abundance than the one observed from the Jungfraujoch (Delbouille). Moreover, for the [OI] 630 nm line there is also a difference between the two intensities: in the Neckel intensity spectrum the line is stronger than in the Delbouille spectrum, even if the effect is less evident. We considered the hypothesis that the difference in height above sea level of the two sites could have induced a higher telluric contribution in the spectra taken at the site of lower elevation. But since there is no evidence of a telluric contribution from the inspection of spectra taken at different air mass, we discarded this hypothesis. More likely, the differences in the spectra might be related to different levels of solar activity at the time of the respective observations (cf. Livingston et al. 2007).

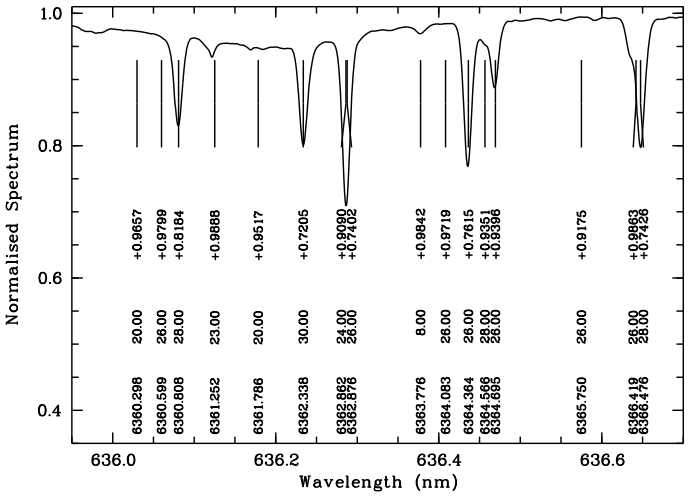

Fig. 6. The Kurucz flux spectrum around the [OI] 636.378 nm line with the identification of the stronger lines.

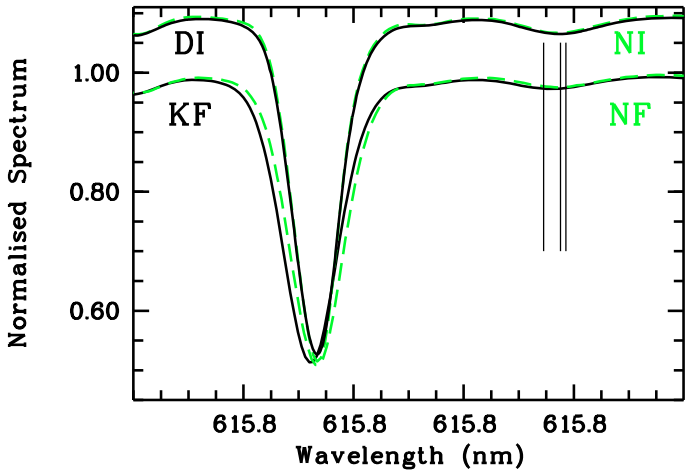

Fig. 7. The O I 615 nm Mult. 10 lines in the four observed spectra used in this work. Symbols are as in Fig. 3. The three vertical lines indicate the laboratory wavelength of the lines.

The fact that the oxygen abundance derived from the two forbidden lines clearly does not agree is disturbing. Obviously, deficiencies in the solar model atmospheres cannot be responsible. In fact, 3D and HM show a similar discrepancy (see Table 3). Presumably, the problem is related to our imperfect knowledge of the blend line contributions. A possible solution is offered by the work of Ayres (2008).

Our adopted oxygen abundance for this line, taking all the measurements into account, is $8.78 \pm (0.05)_{\rm stat} \pm (0.12)_{\rm syst}$, which is $A({\rm O}) = 8.78 \pm 0.12$ (see Table 4 for details).

5.3.3. O I 615 nm

These lines of Mult. 10 lie in a very complex spectral region (see Fig. 7), close to a rather strong iron line and in the range of many CN lines, which make the continuum placement problematic. The *EW* was measured using the de-blending capability of `splot`, with which we accounted for the presence of the neighbouring Fe I line. The *EW* is very sensitive to the placement of the continuum. The oxygen abundance is then obtained from matching this *EW* with the 3D curve-of-growth.

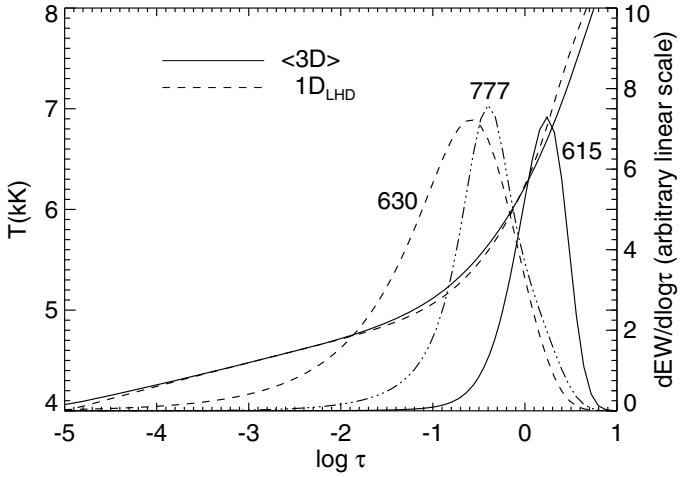

Fig. 8. The average temperature profile (left ordinate) of the 3D model (solid line) and the temperature profile of the 1D$_{\rm LHD}$ model (dashed) are depicted as a function of Rosseland optical depth. The *EW* contribution function of the disc-centre 3D synthetic spectrum (right ordinate) of the 615 nm line (solid), is compared to that of the 630 nm (dashed) and 777 nm (triple dot-dashed) lines. The contribution functions are scaled to have similar maxima and are plotted against their respective monochromatic continuum optical depths.

Our adopted LTE oxygen abundance for this line is 8.63 for the disc-centre spectra and 8.64 for the flux spectra. For both disc-centre and flux we estimate a global systematic error of 0.21 dex, while the statistical error is 0.01 for flux and 0.03 for intensity (see Table 4 for details). We neglect any possible error related to the molecular data because we think they are included in the error associated with the continuum level placement.

The 1D$_{\rm LHD}$ results overestimate the oxygen abundance by about +0.03 dex (flux); in other words, the 3D correction is negative, −0.03 dex. Only for this line do we find a negative 3D correction, and this is a consequence of the effect of horizontal temperature fluctuations, 3D–⟨3D⟩, being appreciable only in this case. This, in turn, is a consequence of the high excitation potential of this line, which implies that it forms in the deep photosphere and is highly sensitive to temperature fluctuations.

Using the Holweger-Müller model, the oxygen abundance is even 0.14 dex higher than the 3D result. For comparison, the corresponding abundance difference is 0.12 dex for ATLAS+WIDTH, and 0.06 dex for MARCS+WIDTH.

Figure 8 shows the *EW* contribution function (following Magain 1986) of the 3D disc-centre synthetic spectrum for the 615.8 nm line in comparison with the 630.0 nm and 777.1 nm lines, together with the temperature structures of the 3D and 1D$_{\rm LHD}$ models. The 615.8 nm line is formed deep inside the photosphere.

For the 1D synthetic spectra we have the possibility of including all the relevant atomic and molecular lines and thus perform line profile fitting. We performed this exercise only on the Kurucz flux: an ATLAS+SYNTHE grid provides $A({\rm O}) = 8.75$. This result is consistent with those based on *EW* measurements as reported above.

The abundance derived from this line is uncertain because the continuum placement is difficult and the atomic parameters of the blend lines in the range are not well known. We note that Holweger (2001) has discarded this line in his analysis of the solar oxygen abundance. We decided to keep it among possible oxygen abundance indicators, although the large associated error gives it a low weight.

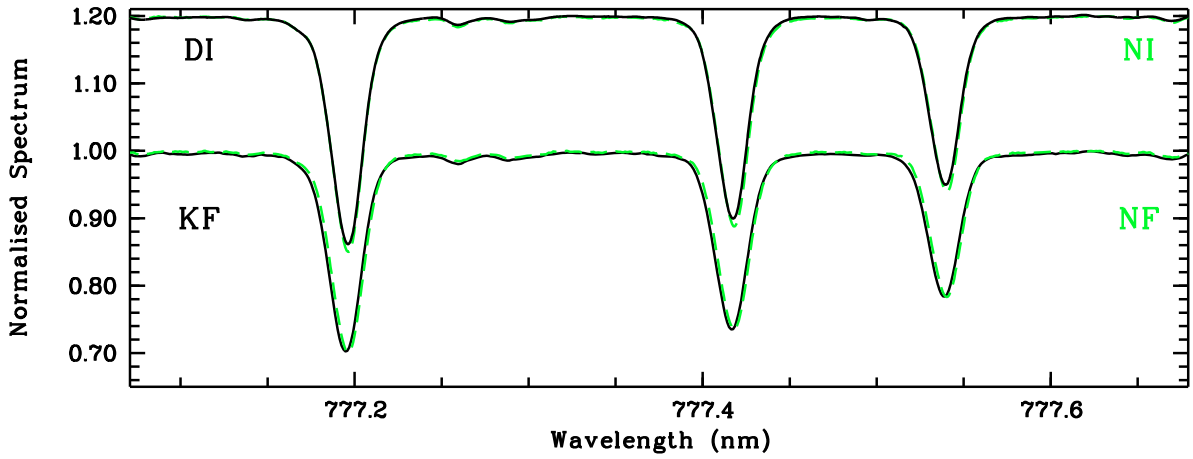

Fig. 9. The O I 777 nm triplet in the four observed spectra used in this work. Symbols are as for Fig. 3.

Table 5. NLTE corrections for all the lines, for different values of S_H, the corrections from Holweger (2001) and A04 for comparison.

line	LTE	NLTE ($S_H = 1$)			NLTE ($S_H = 1/3$)		NLTE ($S_H = 0$)			Flux/Intensity
nm	A(O)	A(O)	corr.	corr. HH[a]	A(O)	corr.	A(O)	corr.	corr. A04[b]	
615.8	8.64	8.64	–0.003		8.64	–0.004	8.64	–0.002	–0.03	F
615.8	8.63	8.62	–0.003	–0.01	8.62	–0.003	8.62	–0.002		I
630.0	8.68	8.68	0.0		8.68	0.0	8.68	0.0		
636.3	8.78	8.78	0.0		8.78	0.0	8.78	0.0		
777.1	9.03	8.87	–0.16		8.81	–0.22	8.75	–0.28	–0.27	F
777.1	8.93	8.85	–0.07	–0.07	8.81	–0.12	8.77	–0.16		I
777.4	8.99	8.84	–0.14		8.79	–0.20	8.74	–0.25	–0.24	F
777.4	8.88	8.80	–0.08	–0.06	8.76	–0.12	8.72	–0.16		I
777.5	8.96	8.85	–0.12		8.80	–0.16	8.75	–0.21	–0.20	F
777.5	8.88	8.82	–0.06	–0.05	8.79	–0.09	8.75	–0.13		I
844.6	8.83	8.75	–0.08		8.72	–0.12	8.68	–0.15	–0.20	F
844.6	8.80	8.75	–0.05		8.72	–0.08	8.70	–0.11		I
926.6	8.74	8.71	–0.03	–0.02	8.69	–0.05	8.65	–0.08	–0.08	I
1130.2	8.75	8.73	–0.01	–0.01	8.72	–0.02	8.71	–0.04		I
1316.4	8.76	8.75	–0.01	–0.01	8.75	–0.01	8.74	–0.02		I

[a] 1D-NLTE correction from Holweger (2001); [b] 3D-NLTE correction from A04.

5.3.4. O I 777 nm triplet

These three strong lines (see Fig. 9) lie in a clean region of the spectrum and do not suffer any blending from other atomic or molecular lines or any telluric absorption. The strength of these lines places them on the saturation part of the curve-of-growth, which, however, is not really flat and still provides a reasonable abundance sensitivity for these lines. The lines have relatively extended wings, such that the wings of neighbouring lines overlap. The *EW* of each line is affected by this effect by 1% to 2.5% (the 777.4 nm line being the most affected). The triplet lines arise from a high excitation level (9.146 eV) and are very sensitive to departures from LTE. From Table 3 it is evident that the *LTE* oxygen abundance obtained from CO^{5}BOLD+Linfor3D for the three lines is greater for the fluxes than for the intensities, which is consistent with the fact that NLTE corrections are greater for flux than for intensity (see Table 5).

The 3D correction (expected to be similar in LTE and NLTE) is about +0.05 dex for flux and +0.10 dex for intensity (assuming a micro-turbulence $\xi = 1.0\,\mathrm{km\,s^{-1}}$). ATLAS+WIDTH implies the same abundances as CO^{5}BOLD+Linfor3D, while the abundances using the MARCS model are 0.06 dex *lower*. Therefore we conclude, as for that of the forbidden lines, that the direction of our 3D correction is *opposite* to what is found by A04 using the MARCS solar model as the 1D reference: while we find A(3D)–A(1D$_{\mathrm{MARCS}}$) = +0.06, they find A(3D)–A(1D$_{\mathrm{MARCS}}$) = −0.06.

Since the lines are on the saturation part of the curve-of-growth, they are sensitive to the micro-turbulence ξ adopted in the 1D analysis. The difference due to a change from 1.0 km s^{-1} to 1.5 km s^{-1} produces a difference of –0.04 dex (for 777.1 nm) in both ⟨3D⟩ and 1D$_{\mathrm{LHD}}$ models.

The fit of the line profile is problematic. The shape of the line is affected by NLTE effects (A04), so even the CO^{5}BOLD+Linfor3D LTE synthetic spectra cannot reproduce the shape of the observed line very well, which is narrower than the synthetic spectra. For this reason our abundance analysis for these lines relies on *EW*s and not on line profile fitting.

Our adopted LTE oxygen abundances for the three lines of the triplet as obtained by matching the measured *EW*s with the 3D curve-of-growth are the following (see Tables 3 and 4 for details). From flux spectra:

$$A(\mathrm{O}) = 9.03 \pm (0.00)_{\mathrm{stat}} \pm (0.12)_{\mathrm{syst}},$$
$$A(\mathrm{O}) = 8.99 \pm (0.01)_{\mathrm{stat}} \pm (0.11)_{\mathrm{syst}},$$
$$A(\mathrm{O}) = 8.96 \pm (0.00)_{\mathrm{stat}} \pm (0.10)_{\mathrm{syst}}.$$

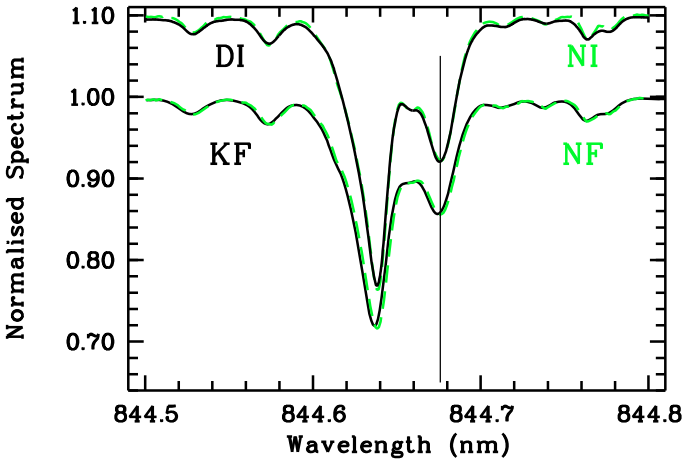

Fig. 10. The O I 844 nm line in the four observed spectra used in this work. Symbols are as for Fig. 3. The vertical line indicates the laboratory wavelength position of the line.

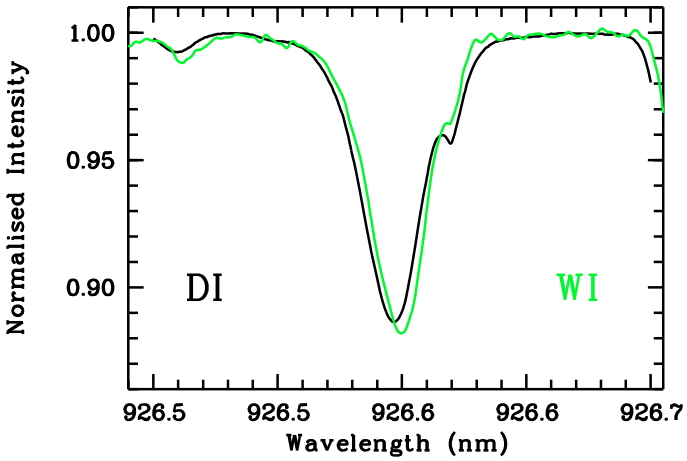

Fig. 11. The observed Delbouille (DI) and Wallace (WI) disc-centre intensity spectra of the O I 926 nm line.

From disc-centre intensity spectra:

$A(\mathrm{O}) = 8.93 \pm (0.01)_{\mathrm{stat}} \pm (0.12)_{\mathrm{syst}}$,
$A(\mathrm{O}) = 8.88 \pm (0.02)_{\mathrm{stat}} \pm (0.11)_{\mathrm{syst}}$,
$A(\mathrm{O}) = 8.88 \pm (0.01)_{\mathrm{stat}} \pm (0.10)_{\mathrm{syst}}$.

5.3.5. O I 844 nm

This line (see Fig. 10) is blended mainly by an iron line for which the atomic data are not well known. Also in this case we tried to divide the observed spectrum by a 1D ATLAS+SYNTHE synthetic one. The spectrum obtained, should only contain oxygen, has a shape that does not agree with the CO^{5}BOLD+Linfor3D synthetic line profile on the blue side, where the Fe I blend line lies, but the agreement is good on the red side.

A de-blending *EW* computation is not always stable, however our "de-blended" *EW* provides an oxygen abundance in the range 8.80 to 8.84, depending on the observed spectrum considered. That an over-plot of the observed spectrum, "as is" with the CO^{5}BOLD+Linfor3D synthetic spectra suggests a value of 8.86 for the oxygen abundance and suggests that a fit with the CO^{5}BOLD+Linfor3D grid avoiding the blue wing gives $A(\mathrm{O}) = 8.80$, indicates that our *EW* is nevertheless useful for the abundance determination (see Table 3). The 3D correction is +0.03 dex for flux and +0.07 dex for disc-centre intensity ($\xi = 1.0\,\mathrm{km\,s^{-1}}$).

Using a 1D ATLAS+SYNTHE grid, we fitted both the observed Kurucz flux spectrum "as is" and the "divided-out" spectrum containing only the oxygen line (obtained by dividing by a synthetic spectrum of only the blend lines), and obtained $A(\mathrm{O}) = 8.79$ and 8.73, respectively. Using a 1D HM+SYNTHE grid in the same way, we obtained instead $A(\mathrm{O}) = 8.82$ and 8.76, respectively.

Our adopted LTE oxygen abundance from this line is: $A(\mathrm{O}) = 8.83 \pm (0.00)_{\mathrm{stat}} \pm (0.33)_{\mathrm{syst}}$ from the flux spectra, and $A(\mathrm{O}) = 8.80 \pm (0.02)_{\mathrm{stat}} \pm (0.33)_{\mathrm{syst}}$ from disc-centre intensity spectra (see Table 4 for details).

5.3.6. O I 926 nm

In the Kurucz flux spectrum, as in the Neckel flux and intensity spectra, the O I 926 nm line is contaminated by a telluric line. The intensity spectra of Delbouille (see Fig. 11) and Wallace have been processed to subtract the telluric contribution. The subtraction is probably not completely successful, since the profile still shows some distortion. Nevertheless, the spectra can be fitted reasonably well. Although the Delbouille spectrum has a higher signal-to-noise (about 5000), the Wallace spectrum (S/N about 500) shows less residual distortion after the subtraction of the telluric line. For this reason the *EW* was only computed from the Wallace intensity spectrum, providing an oxygen abundance of $A(\mathrm{O}) = 8.75$ in 3D. The 3D correction in this case is +0.06 dex ($\xi = 1.0\,\mathrm{km\,s^{-1}}$).

We also did line-fitting restricted to a range that excludes the portion of the line that is affected by the telluric absorption. The fit of the Delbouille spectrum with a CO^{5}BOLD+Linfor3D grid gives $A(\mathrm{O}) = 8.67$. The 3D fitting of the Wallace spectrum results in $A(\mathrm{O}) = 8.71$. Fitting the Delbouille and Wallace spectra with an ATLAS+SYNTHE grid, we obtain $A(\mathrm{O}) = 8.68$ and 8.66, respectively. With the Holweger-Müller+SYNTHE grid, we have instead $A(\mathrm{O}) = 8.74$ and 8.73, respectively[9].

For this line our adopted LTE oxygen abundance is $A(\mathrm{O}) = 8.74 \pm (0.01)_{\mathrm{stat}} \pm (0.12)_{\mathrm{syst}}$ (see Table 4 for details).

5.3.7. O I 1130 nm

In the Kurucz flux atlas and in both Neckel spectra, the O I 1130 nm line is blended by a telluric absorption. The Wallace intensity spectrum has been cleaned from telluric absorption, but its S/N is only about 80, inferior to the Kitt Peak FTS scans we considered, and insufficient for our purposes.

Our analysis of this line therefore relies on a special reduction of FTS scans obtained from the NSO Digital Archive (see Fig. 12). The O I 1130 nm line, and the companion 1316 nm multiplet described below, fall in the shoulders of very strong telluric absorptions and require a careful correction for the blending. One of us (TRA) examined the NSO/FTS catalogue of observations and identified a suitable series of scans, taken on the 13th and 14th of September 1983. Each scan was a co-add of two interferograms totalling 5 minutes exposure, through a 5″ diameter aperture, at disc-centre. The datasets are listed as "8309NNr0.XXX" where "NN" is the day (13 or 14), and "XXX" is a scan number. Hereafter, these will be described as

[9] Note, that the values given in Table 3 differ from the values here since they are based on matching the line *EW*, not line profile fitting.

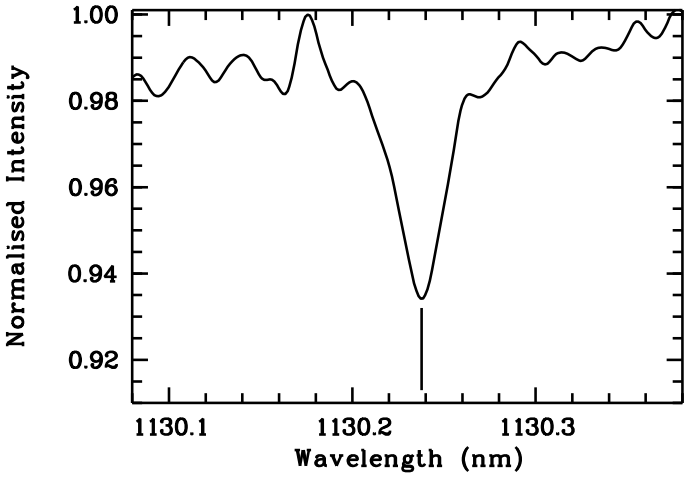

Fig. 12. The observed disc-centre intensity spectrum used for the O I 1130 nm line. The vertical line indicates the laboratory wavelength position of the line.

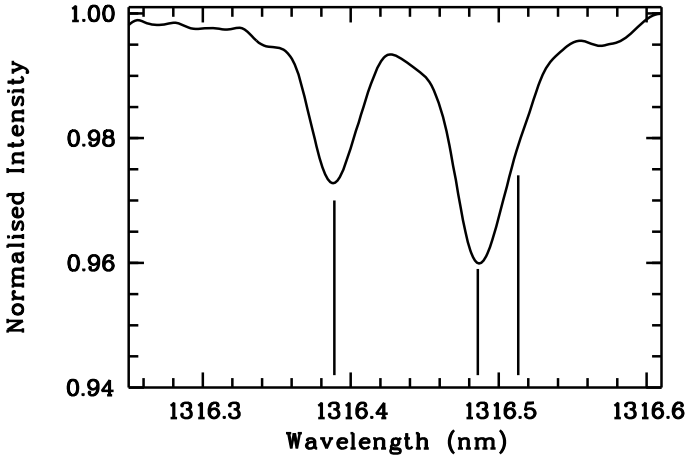

Fig. 13. The observed disc-centre intensity spectrum used for the analysis of the O I 1316 nm line. The vertical lines indicate the laboratory wavelengths of the three O I lines discussed in the text.

"NN.XXX' for simplicity. Scan 13.004 was taken in the early morning at about 09:00 local time, at a moderate airmass of 1.7. Scan 13.011 was acquired close to local noon at a low airmass of 1.14. Scan 13.015 was taken later in the afternoon, again at a moderate airmass of 1.5. On the following day, scan 14.007 was collected at about 09:00 local time at an airmass of 1.7, while scan 14.010 was taken about an hour before local noon, at a lower airmass of 1.27. The spectral resolution of these data is very high, around 2×10^5, and the S/N is very high as well, $>10^3$, taking only the Poisson noise into account and ignoring other sources of uncertainty. Owing to the excellent frequency stability of the FTS scans, pairs taken at low and high airmass can be registered very precisely to the telluric absorptions, and ratioed to eliminate the solar component. The ratio can be modelled as an exponential attenuation factor, and then applied back to the observed spectra as a correction for the telluric component. By subjecting this technique to various combinations of the low and high airmass scans, one can average over slight variations in the atmospheric attenuation factor in the morning versus the afternoon (owing, say, to increases in the humidity due to solar heating), and possible slight changes in the solar component due to 5 min oscillations, convection, and the like. All these effects contribute to the deterioration of the information content of the spectrum and may be effectively thought of as "noise". This source of noise is in fact much more than the pure Poisson noise in the spectrum. The dispersion in the derived solar profiles is a rough measure of the uncertainty of the telluric correction procedure and of intrinsic solar variations. For the O I 1130 nm line, the corresponding S/N is about 15. We refer to this S/N ratio as "equivalent S/N".

The line is blended with a weaker iron line at $\lambda = 1130.242$ nm, $\log gf = -2.381$ from Kurucz's Cowan-code computations, whose contribution is 17% (for an ATLAS+SYNTHE synthetic spectrum with $A(\mathrm{O}) = 8.60$) to the complete EW of the blend. From fitting with a CO^{5}BOLD+Linfor3D grid we derived an oxygen abundance of $A(\mathrm{O}) = 8.76$. The corresponding value obtained from fitting with ATLAS+SYNTHE is $A(\mathrm{O}) = 8.75$. The EW-based abundance determination gives a fully consistent result, $A(\mathrm{O}) = 8.75$. The 3D correction is +0.04 dex ($\xi = 1.0\,\mathrm{km\,s^{-1}}$). Our adopted LTE oxygen abundance for this line is: $A(\mathrm{O}) = 8.75 \pm (0.01)_{\mathrm{stat}} \pm (0.17)_{\mathrm{syst}}$ (see Table 4 for details).

5.3.8. O I 1316 nm

As shown in Fig. 13, three oxygen lines can be found in this multiplet, at λ 1316.3889 nm, 1316.4858 nm, and 1316.5131 nm. The strongest one (1316.4858 nm) is blended with one of the other oxygen lines (1316.5131 nm). For the three lines we adopt for $\log gf$ values of −0.28, −0.250, −0.728, respectively, according to Biémont et al. (1991).

The Wallace intensity solar spectrum has an S/N of about 700, but the spectrum is poorly rectified, making the continuum placement very uncertain. We decided not to use this spectrum but rather the Kitt Peak FTS scans mentioned above (Sect. 5.3.7), which have a higher S/N ($>10^3$) and are well-rectified. For the 1316 nm feature the equivalent S/N for the strongest of the lines, having a central depth of about 5%, is about 25, somewhat higher than for the 1130 nm line. From fitting this spectrum, we obtain $A(\mathrm{O}) = 8.75$ with a 3D grid for all three lines. With an ATLAS+SYNTHE grid, the fit gives $A(\mathrm{O}) = 8.77$.

For this line our LTE adopted abundance is $A(\mathrm{O}) = 8.76 \pm (0.01)_{\mathrm{stat}} \pm (0.22)_{\mathrm{syst}}$.

6. Discussion and conclusions

The best estimate of the solar oxygen abundance is obtained by a suitable average of the abundances derived from the individual lines. Our adopted oxygen abundances are summarised in Table 4, together with associated errors, while corrections for departures from LTE are listed in Table 5. A different choice in the collision efficiency with H-atoms, quantified by the scaling factor S_{H} (see Sect. 5.1), produces a different value in the solar oxygen abundance. A weighted mean

$$\mu = \frac{\Sigma\left(x_i/\sigma_i^2\right)}{\Sigma\left(1/\sigma_i^2\right)} \qquad \sigma_\mu^2 = \frac{1}{\Sigma\left(1/\sigma_i^2\right)} \tag{1}$$

(Bevington & Robinson 1992, p. 59), using the total errors from Table 4, provides an oxygen abundance of

$$\begin{array}{llll} A(\mathrm{O}) = & 8.73 \pm 0.04 & \text{for} & S_{\mathrm{H}} = 0, \\ A(\mathrm{O}) = & 8.76 \pm 0.04 & \text{for} & S_{\mathrm{H}} = 1/3, \\ A(\mathrm{O}) = & 8.79 \pm 0.04 & \text{for} & S_{\mathrm{H}} = 1. \end{array} \tag{2}$$

Our preference is an intermediate value, $S_{\rm H} = 1/3$, so that the solar oxygen abundance we advocate is $A({\rm O}) = 8.76 \pm 0.04 \pm 0.03$. The first error includes the statistical uncertainties, as well as any systematic uncertainty, except the one related to the NLTE corrections, which are considered separately to be 0.03 dex. If we sum the two errors, we arrive at an oxygen abundance of $A({\rm O}) = 8.76 \pm 0.07$. Computing A(O) from the simple average, instead of taking the weighted mean, we only obtain slightly smaller abundances. Oxygen abundances derived from intensity spectra are systematically smaller than those obtained from flux spectra, but the difference is less than 0.04 dex.

If we consider the NLTE abundance in column 6 of Table 5, corresponding to $S_{\rm H} = 1/3$, excluding the 615 nm line, we find a line to line scatter of 0.13 dex, so compatible with the 1σ error bars we attribute to the individual lines. The same range in A(O) is obtained for $S_{\rm H} = 0$. The 615 nm line requires a lower abundance and would increase the overall scatter, but, as we discussed in the section devoted to this line, this line is particularly problematic.

The lowest abundance after the 615 nm line is coming from the forbidden oxygen line at 630 nm. The relatively low oxygen abundance it implies is sensitive to the abundance of nickel, which we *assumed* to be 6.25, the presently recommended value. Had we adopted the equivalent width of 4.3 pm, which A04 attribute to the oxygen contribution to the 630 nm line, we would have obtained $A({\rm O}) = 8.78$, moving the result closer to the other lines and becoming fully consistent with forbidden oxygen line at 636 nm.

We do not show comparisons between line profile shapes of synthetic and observed spectra because we cannot reproduce the observed features due to blends, as is the case for the 636, 844, and 926 nm lines; the triplet is affected by NLTE corrections. Since our NLTE computation is based on the $\langle$3D$\rangle$ model, we cannot reproduce the profile of the triplet lines accurately. The infrared lines, after correction for telluric absorption, have low S/N so that visual comparison to synthetic profiles is not particularly illuminating. Only for the 630 nm forbidden line can the observed line profile shape be compared to the synthetic 3D spectrum, and this is shown in Fig. 5 for all four observed profiles.

Our results must be compared with those of Holweger (2001), A04, and to the one of Ayres (2008). Holweger (2001) provides $A({\rm O}) = 8.736 \pm 0.078$, thus ~0.05 dex lower than our weighted mean for $S_{\rm H} = 1$, right within one σ of his error bar. The mean oxygen abundance obtained from the atomic lines by A04, A(O)=8.65, and our weighted mean, for $S_{\rm H} = 0$, differ of +0.08 dex.

One of us (Ayres 2008) has recently carried out an independent analysis specifically of the 630 nm O I forbidden line, taking a different approach than followed in the present work. Here, we have allowed the wavelength scale in the vicinity of the 630 nm feature to float, to accommodate the Ni I blend at its nominal abundance. With this approach we obtain an excellent match to the observed line-shape, although Ni I accounts for a larger fraction of the equivalent width of the full feature (see Fig. 4) than would be inferred from the original analysis of the forbidden oxygen line by Allende Prieto et al. (2001, their Fig. 1). Curiously, we obtain nearly the same oxygen abundance as Allende Prieto et al. (2001), even though here the O I component occupies a smaller fraction of the full equivalent width. At the time Allende Prieto et al. (2001) performed their analysis, the oscillator strength of the Ni transition was not known precisely, and they left the product $gf\epsilon$(Ni) as a free fitting parameter. They obtained a contribution corresponding to a low nickel abundance of A(Ni) = 6.05, i.e. a rather small contribution, using today's accepted value of the oscillator strength of the Ni transition. It is conceivable that the difficulty in the continuum placement are responsible for the disparate findings.

Ayres (2008) took the alternative fitting approach of fixing the wavelength scale and allowing the Ni I abundance to float. Although the absolute velocity calibrations of the solar atlases and specially reduced spectra we have described earlier can be uncertain by hundreds of m s^{-1}, Ayres circumvented that deficiency by adjusting an observed FTS spectrum to match 3D-synthesised cores of several Fe I absorption lines in the immediate vicinity of the [O I] 630 nm feature (the 3D model was a single CO^{5}BOLD snapshot in this case). This procedure moves the blend bluewards of the result we obtained here, leading to a higher fraction of the equivalent width contributed by O I, and lowering the fraction of Ni I (by about 30%). The inferred oxygen abundance is larger than obtained here, $A({\rm O}) = 8.81 \pm 0.04$. Ayres's approach relies on an accurate prediction of the relative core velocities of the Fe I and O I (+ Ni I) features by the 3D model, and assumes that the Ni I abundance can be treated as a free parameter.

In both cases, it is important to note that the CO^{5}BOLD model provides a different conversion between fractional O I equivalent width and inferred oxygen abundance than the 3D simulations reported by Allende Prieto et al. (2001) and subsequent studies also using the Stein-Nordlund class of models. The differences might be related to the different temperature gradients of the 3D models (e.g., as exhibited by the 1D average stratifications shown in Fig. 1) since a main factor governing the strength of a weak photospheric line is the temperature gradient in the line formation zone. Another factor introducing systematic uncertainties is the spectral synthesis. Meléndez (2004) applied the spectral synthesis code MOOG (Sneden 1973) in his determination of the solar oxygen abundance. Besides mainly targeting OH molecular lines in the infrared, he recalculated the oxygen abundance from the forbidden oxygen line at 630 nm based on the average 3D model of A04 and their equivalent width, as well as oscillator strength, obtaining $A({\rm O}) = 8.75$. According to our calculations, horizontal temperature fluctuations have essentially no effect on the resulting equivalent width of the line in disc-integrated spectra so that Meléndez' value can be directly compared to the value of 8.69 quoted by A04. We are left with the uncomfortable conclusion that differences in the spectral synthesis can introduce differences as large as 0.06 dex in the derived oxygen abundance.

The weighted mean of the abundances derived from several O I lines in the solar spectrum implies a solar oxygen abundance in the range $A({\rm O}) = 8.73$ to $A({\rm O}) = 8.79$, depending on the actual influence of collisions by neutral hydrogen atoms on the NLTE level populations of oxygen. The lower abundance is obtained by a total neglect of such collisions, the higher abundance is obtained by assuming the rather large cross sections provided by the recipe of Steenbock & Holweger (1984), which may be considered an upper limit to the efficiency of these collisions. Any treatment of neutral hydrogen collisions intermediate between these two extremes will provide an oxygen abundance in the above range.

Apart from this systematic uncertainty of the NLTE corrections, we regard the determination of A(O) as very robust, with a total error in the weighted mean of 0.07 dex. Considering our present ignorance on the actual role of collisions by neutral hydrogen, we believe that it is reasonable to assume that the true value lies somewhere in between these two extreme assumptions. Therefore, assuming $S_{\rm H} \approx 1/3$, our recommended

value for the solar oxygen abundance is the mean of the two, $A(\mathrm{O}) = 8.76 \pm 0.07$.

Our recommended oxygen abundance is a downward revision with respect to that of Grevesse & Sauval (1998). Using that set of solar abundances the solar metallicity is $Z_\odot = 0.017$. If we take that set of solar abundances and change only the oxygen abundance to our recommended value, $Z_\odot$ drops to 0.016. On the other hand, our oxygen abundance is an upward revision relative to what was recommended by A04. By taking the solar abundances of Asplund et al. (2005) but our oxygen abundance, we find $Z_\odot = 0.014$. Clearly the latter result is influenced by the general downward revision of all the solar abundances advocated by Asplund and collaborators. Having found a higher solar oxygen abundance by using CO^{5}BOLD models, and having been unable to confirm the downward revision of phosphorus (Caffau et al. 2007b) and sulphur (Caffau & Ludwig 2007; Caffau et al. 2007a), it seems not unlikely that, also for other elements, a CO^{5}BOLD based analysis would imply higher abundances than recommended by Asplund et al. (2005).

We should compare our result with solar oxygen abundances deduced by other means. Delahaye & Pinsonneault (2006) obtain $A(\mathrm{O}) = 8.86 \pm 0.041 \pm 0.025$ (CNNe) from the seismic properties; the latter uncertainty is related to the abundance of C, N, and Ne. Antia & Basu (2006) using the helioseismically measured sound speed profile obtained $Z = 0.0172 \pm 0.002$, but the method does not permit the abundance of a single element to be deduced. Chaplin et al. (2007) using the frequencies of low-degree acoustic oscillations of the Sun obtained Z in the range 0.0187–0.0229. Basu & Antia (2008) find $Z = 0.016$, again from helioseismic considerations. As we can see, all the results obtained from the properties of the solar interior favour a "high" solar metallicity, and therefore a "high" oxygen abundance. In the same line are the results obtained in the work of Turck-Chièze et al. (2004): they find a better agreement when they compare the seismic model ($Z = 0.017$) to the solar model with the abundances of Holweger (2001) ($Z = 0.015$) with respect to the model with A04 abundances ($Z = 0.012$).

The downward revision of the solar Z by Asplund et al. (2005) is generally considered to mainly stem from the use of 3D models, as opposed to 1D models used in older analysis (e.g. Allende Prieto 2007). The result of our analysis reveals, however, that this is not the case at least for oxygen. The 3D corrections for the O I lines are small, and for all lines, except for the 615.8 nm line, they are *positive*, indicating that the 3D model provides a *higher* abundance than the corresponding 1D$_{\mathrm{LHD}}$ model (see Table 3). The average 3D correction, if we consider all the oxygen lines, is +0.049 assuming a microturbulence $\xi = 1.0\,\mathrm{km\,s^{-1}}$ in the 1D$_{\mathrm{LHD}}$ model, and +0.066 when $\xi = 1.5\,\mathrm{km\,s^{-1}}$.

Closer inspection shows that the lower oxygen abundance of A04 is essentially a result of using lower equivalent widths, on average, and of the choice of $S_{\mathrm{H}} = 0$ (larger NLTE corrections), which are both acting in the downward direction. The differences between the Stein & Nordlund model employed by A04 and our CO^{5}BOLD model (see Fig. 1) are not essential for the resulting oxygen abundance. The fact that our oxygen abundance with $S_{\mathrm{H}} = 0$ is 0.08 dex higher is entirely due to our measured equivalent widths, which are larger. If we use the CO^{5}BOLD model and the equivalent widths of A04, we find $A(\mathrm{O}) = 8.67$ when averaging the oxygen abundances for the atomic lines, very close to their result. Therefore, the 3D corrections quoted by A04 are in the opposite direction to ours due to the different choice of 1D reference model.

A04 argued that their suggested low O abundance would place the Sun on the same oxygen level as is observed in the local interstellar medium and nearby B stars. However, it is not at all obvious that the Sun's chemical composition should reflect its immediate surroundings since it might have migrated towards larger galactic radii from its place of formation (Wielen et al. 1996) of higher metallicity. Moreover, the Sun harbours a planetary system, and it is now well-established that planet-hosting stars have, on average, higher metallicities than stars with no planets. Ecuvillon et al. (2006) present a uniform analysis of oxygen abundances in a volume-limited sample of 59 stars with no planets and compare it to a sample of 96 planet-hosting stars. The mean oxygen abundance of the sample of planet-hosting stars is 8.77, while the mean oxygen abundance of the sample of stars with no planets is 8.67. Thus our recommended solar oxygen abundance places the Sun in a very popular position among planet-hosting stars in the solar neighbourhood.

To improve our knowledge of the solar oxygen abundance, one should focus in the first place on the collisions with hydrogen atoms, both theoretically and experimentally. To the readers who have been following the saga of the solar abundances for some time it is perhaps not surprising to find that the measurement of high accuracy equivalent widths is still an open issue. One should try to better constrain the placement of the continuum, and the influence of the blending lines.

Acknowledgements. This paper is dedicated to the late Hartmut Holweger who accompanied the initial phases of the oxygen project with encouragement and advice. We thank Sveneric Johansson for his input on the isotopic splitting of nickel lines. We are grateful to Martin Asplund for providing us with the full details of his analysis. Furthermore, we are grateful to Robert Kurucz for providing the revised version of his solar flux atlas. We wish to thank Rosanna Faraggiana for many fruitful discussions on the topic of abundance determinations. Special thanks also go to Inga Kamp for giving us the Kiel code and the oxygen model atom and helping us in their use. E.C., H.G.L., and P.B. acknowledge support from EU contract MEXT-CT-2004-014265 (CIFIST).

References

Allende Prieto, C. 2007, Invited review to appear in the Proceedings of the 14th Cambridge Workshop on Cool Stars, Stellar Systems, and the Sun, ed. G. van Belle, Pasadena, November 2006 [arXiv:astro-ph/0702429]
Allende Prieto, C., & Garcia Lopez, R. J. 1998, A&AS, 131, 431
Allende Prieto, C., Lambert, D. L., & Asplund, M. 2001, A&A, 556, 63
Allende Prieto, C., Asplund, M., & Fabiani Bendicho, P. 2004, A&A, 423, 1109
Anders, E., & Grevesse, N. 1989, Geochim. Cosmochim. Acta, 53, 197
Anstee, S. D., & O'Mara, B. J. 1995, MNRAS, 276, 859
Antia, H. M., & Basu, S. 2006, ApJ, 644, 1292
Asplund, M., Grevesse, N., Sauval, A. J., Allende Prieto, C., & Kiselman, D. 2004, A&A, 417, 751
Asplund, M., Grevesse, N., & Sauval, A. J. 2005, Cosmic Abundances as Records of Stellar Evolution and Nucleosynthesis, ASP Conf. Ser., 336, 25
Ayres, T. R. 2008, ApJS, submitted
Ayres, T. R., Plymate, C., & Keller, C. U. 2006, ApJS, 165, 618
Bahcall, J. N., Basu, S., Pinsonneault, M., & Serenelli, A. M. 2005a, ApJ, 618, 1049
Bahcall, J. N., Serenelli, A. M., & Basu, S. 2005b, ApJ, 621, L85
Barklem, P. S., & O'Mara, B. J. 1997, MNRAS, 290, 102
Barklem, P. S., O'Mara, B. J., & Ross, J. E. 1998a, MNRAS, 296, 1057
Barklem, P. S., Anstee, S. D., & O'Mara, B. J. 1998b, Publ. Astron. Soc. Austr., 15, 336
Basu, S., & Antia, H. M. 2008, Phys. Rep., 457, 217
Bensby, T., Feltzing, S., & Lundström, I. 2004, A&A, 415, 155
Bevington, P. R., & Robinson, D. K. 1992, Data reduction and error analysis for the physical sciences, 2nd edn. (New York: McGraw-Hill)
Biémont, E., Hibbert, A., Godefroid, M., Vaeck, N., & Fawcett, B. C. 1991, ApJ, 375, 818
Caffau, E., Bonifacio, P., Faraggiana, R., et al. 2005, A&A, 441, 533
Caffau, E., & Ludwig, H.-G. 2007, A&A, 467, L11
Caffau, E., Faraggiana, R., Bonifacio, P., Ludwig, H.-G., & Steffen, M. 2007a, A&A, 470, 699
Caffau, E., Steffen, M., Sbordone, L., Ludwig, H.-G., & Bonifacio, P. 2007b, A&A, 473, L9

Castelli, F. 2005, Mem. Soc. Astron. Ital. Suppl., 8, 44
Cayrel, R. 1988, The Impact of Very High S/N Spectroscopy on Stellar Physics, IAU Symp., 132, 345
Cayrel, R., Steffen, M., Chand, H., et al. 2007, A&A, 473, L37
Chaplin, W. J., Serenelli, A. M., Basu, S., et al. 2007, ApJ, 670, 872
Delahaye, F., & Pinsonneault, M. H. 2006, ApJ, 649, 529
Delbouille, L., Roland, G., & Neven, L. 1973, Institut d'Astrophysique, Liège: Université de Liège
Delbouille L., Roland G., Brault, & Testerman 1981, Photometric atlas of the solar spectrum from 1850 to 10 000 cm^{-1}, http://bass2000.obspm.fr/solar_spect.php
Drawin, H.W. 1969, Z. Physik, 225, 483
Ecuvillon, A., Israelian, G., Santos, N. C., et al. 2006, A&A, 445, 633
Freytag, B., Steffen, M., & Dorch, B. 2002, Astron. Nachr., 323, 213
Freytag, B., Steffen, M., Wedemeyer-Böhm, S., & Ludwig, H.-G. 2003, CO5BOLD User Manual, http://www.astro.uu.se/~bf/co5bold_main.html
Gehren, T., Korn, A. J., & Shi, J. 2001, A&A, 380, 645
Gray, D. F. 2005, The Observation and Analysis of Stellar Photospheres, 3rd edition, ed. D. F. Gray (UK: Cambridge University Press), http://www.cambridge.org/us/catalogue/catalogue.asp?isbn=0521851866. Cambridge
Grevesse, N., & Sauval, A. J. 1998, Space Sci. Rev., 85, 161
Gustafsson, B., Edvardsson, B., Eriksson, K., et al. 2003, Stellar Atmosphere Modeling, 288, 331
Gustafsson, B., Heiter, U., & Edvardsson, B. 2007, IAU Symp., 241, 47
Guzik, J. A., Watson, L. S., & Cox, A. N. 2006, Mem. Soc. Astron. Ital., 77, 389
Holweger, H. 1967, Z. Astrophys., 65, 365
Holweger, H. 2001, Joint SOHO/ACE workshop, Solar and Galactic Composition, AIP Conf. Proc., 598, 23
Holweger, H., & Müller, E. A. 1974, Sol. Phys., 39, 19
Kurucz, R. 1993a, ATLAS9 Stellar Atmosphere Programs and 2 km/s grid, Kurucz CD-ROM No. 13, Cambridge, Mass.: Smithsonian Astrophysical Observatory
Kurucz, R. 1993b, SYNTHE Spectrum Synthesis Programs and Line Data, Kurucz CD-ROM No. 18, Cambridge, Mass.: Smithsonian Astrophysical Observatory
Kurucz, R. L. 2005a, Mem. Soc. Astron. Ital. Suppl., 8, 189
Kurucz, R. L. 2005b, Mem. Soc. Astron. Ital. Suppl., 8, 14
Johansson, S., Litzén, U., Lundberg, H., & Zhang, Z. 2003, ApJ, 584, L107
Lambert, D. L. 1978, MNRAS, 182, 249
Livingston, W., Wallace, L., White, O.R., & Giampapa, M. S. 2007, ApJ, 657, 1137
Ludwig, H.-G. 1992, Ph.D. Thesis, Univ. Kiel
Ludwig, H.-G., Jordan, S., & Steffen, M. 1994, A&A, 284, 105
Ludwig, H.-G., Steffen, M., Freytag, B., et al. 2008, A&A, in preparation
Magain, P. 1986, A&A, 163, 135
Meléndez, J. 2004, ApJ, 615, 1042
Neckel, H. 1999, Sol. Phys., 184, 421
Neckel, H., & Labs, D. 1984, Sol. Phys., 90, 205
Nordlund, Å. 1982, A&A, 107, 1
Paunzen, E., et al. 1999, A&A, 345, 597
Pierce, A. K. 1964, Appl. Opt., 3, 1337
Ralchenko, Y. 2005, Mem. Soc. Astron. Ital. Suppl., 8, 96
Rosberg, M., Litzen, U., & Johansson, S. 1993, MNRAS, 262, L1
Ryan, S. G. 1998, A&A, 331, 1051
Sbordone, L. 2005, Mem. Soc. Astron. Ital. Suppl., 8, 61
Sbordone, L., Bonifacio, P., Castelli, F., & Kurucz, R. L. 2004, Mem. Soc. Astron. Ital. Suppl., 5, 93
Sneden, C. 1973, Ph.D. Thesis, Univ. Texas
Socas-Navarro, H., & Norton, A. A. 2007, ApJ, 660, L153
Solanki, S. K., & Steenbock, W. 1988, A&A, 189, 243
Steenbock, W., & Holweger, H. 1984, A&A, 130, 319
Storey, P. J., & Zeippen, C. J. 2000, MNRAS, 312, 813
Stürenburg, S., & Holweger, H. 1990, A&A, 237, 125
Stürenburg, S., & Holweger, H. 1991, A&A, 246, 644
Turck-Chièze, S., Couvidat, S., Piau, L., et al. 2004, Phys. Rev. Lett., 93, 211102
Vögler, A., Bruls, J. H. M. J., & SchÃijssler, M. 2004, A&A, 421, 741
Wallace, L., Livingston, W., Hinkle, K., & Bernath, P. 1996, ApJS, 106, 165
Watson, L. S., & Guzik, J. A. 2006, Mem. Soc. Astron. Ital. Suppl., 77, 154
Wedemeyer, S., Freytag, B., Steffen, M., Ludwig, H.-G., & Holweger, H. 2004, A&A, 414, 1121
Wielen, R., Fuchs, B., & Dettbarn, C. 1996, A&A, 314, 438